SEGREGATION IN A Cu BICRYSTAL

by

Charl Jeremy Jafta

A thesis presented in fulfilment of the requirements of the degree

MAGISTER SCIENTIAE

In the faculty of Natural and Agricultural Sciences,

Department of Physics

at the University of the Free State

Republic of South Africa

Study leader: **Prof. W. D. Roos**

Co-Study leader: **Prof. J. J. Terblans**

November 2010

I dedicate this dissertation to my father

Peter Jafta

(1949 – 2009)

"He heals the broken hearted and binds up their wounds" (Psalm 147:3)

Acknowledgements

The author wishes to express his sincere appreciation to the following:

Key words

Cu (Copper) bi-crystal

(111) surface orientation

(110) surface orientation

Sb – Antimony

Bi – Bismuth

Annealing system

AES modification

Grain boundary

AES – Auger Electron Spectroscopy

XPS – X-ray Photo-electron Spectroscopy

XRD – X-ray Diffraction

SEM – Secondary Electron Microscopy

Abstract

A literature study showed that the rate of segregation to a Cu(110) surface is higher than to a Cu(111) surface. The difference is mainly due to a change in the vacancy formation energy which determines the diffusion coefficient. The diffusion coefficient is a very important factor during kinetic segregation and determines the flux of atoms to the surface.

The experimental verification of the calculations is very difficult due to the high number of parameters involved during measurements.

In this study, the segregation parameters for Sb in a Cu bi-crystal, with (111) and (110) surface orientations, were determined. A unique experimental setup and measuring procedure was used to determine the concentration of the segregant as a function of temperature. This setup ensures exactly the same experimental conditions for both orientations allowing the researcher to directly compare the segregation parameters.

The Auger Electron Spectroscopy (AES) spectrometer, used to measure the Sb enrichment on the Cu bi-crystal surfaces, was specially modified for these measurements. The deflection plates in the primary e$^-$ gun were physically aligned, horizontally and vertically, relative to the laboratory frame of reference. A computer program was developed to control the deflection of the e$^-$ beam during the measurements.

Because it was decided on diffusional doping of the crystal an annealing system was designed and built. The system is consistently successful in annealing specimens at high temperatures for long periods of time in non corrosive atmospheres. Because of concerns that the grain boundary can influence the segregation, a secondary study was done on the migration of grain boundaries in polycrystalline Cu specimens. These studies indicate the inhibition of grain boundary mobility with small additions of Sb.

6

The concentration build up on both surface orientations was monitored while the crystal was heated linearly with time, at different rates. The experimental data were fitted using the Modified Darken Model. The extracted Sb segregation parameters, in the Cu(110) surface are $D_0 = 2.2 \times 10^{-5}(\pm 5\%)$ m^2.s^{-1}, $Q = 196 \pm 2$ kJ.mol^{-1}, $\Delta G = -90 \pm 1$ kJ.mol^{-1} and $\Omega_{CuSb} = -5 \pm 1$ kJ.mol^{-1}, and in the Cu(111) surface are $D_0 = 1.1 \times 10^{-3}(\pm 5\%)$ m^2.s^{-1}, $Q = 233 \pm 2$ kJ.mol^{-1}, $\Delta G = -89 \pm 1$ kJ.mol^{-1} and $\Omega_{CuSb} = -3 \pm 1$ kJ.mol^{-1}.

With the experimental conditions kept constant for both surface orientations, it is seen that there is a definite change in the pre-exponential factor and activation energy which compares well with values in literature. The different pre-exponential factors allows the opportunity to calculate, for the first time, the difference in the change in entropy ($\Delta S_{\Delta s}$) for the two surface orientations as 36 J.mol^{-1}K^{-1}.

A unique custom build annealing system and experimental method used in this study proved to be highly successful and a change in the Sb segregation parameters, as a function of surface orientation, were experimentally verified.

Opsomming

'n Literatuur studie het gewys dat die tempo van segregasie na 'n Cu(110) oppervlak hoër is as in die geval van 'n Cu(111) oppervlak. Hierdie verskil is hoofsaaklik as gevolg van die verskil in die leemtevormingsenergie wat die diffusiekoeffisiënt bepaal. Die diffusiekoeffisiënt is 'n belangrike faktor tydens die kinetika van segregasie en bepaal die vloed van atome na die oppervlak.

Om die berekeninge eksperimenteel te bevestig is baie moeilik, as gevolg van die groot aantal veranderlikes betrokke wanneer metings gedoen word.

In hierdie studie is die segregasie parameters vir Sb in 'n Cu bikristal, met (111) en (110) oppervlakoriëntasies, bepaal. 'n Unieke eksperimentele opstelling en meetprosedure was gebruik om die konsentrasie van die segregant as 'n funksie van temperatuur te bepaal. Hierdie opstelling verseker presies dieselfde eksperimentele kondisies vir beide die oppervlakoriëntasies, wat dan toelaat dat die segregasie parameters direk met mekaar vergelyk kan word.

Die Auger-elektronspektroskopie (AES) spektrometer wat gebruik is om die Sb verryking op die Cu bikristal oppervlaktes te meet, is spesiaal gemodifiseer vir hierdie metings. Die defleksieplate in die primêre e⁻ geweer was fisies horisontaal en vertikaal opgelyn, relatief tot die laboratorium se verwysingsraamwerk. 'n Rekenaar program is ontwikkel om die defleksie van die e⁻ bundel te beheer tydens metings.

'n Uitgloeisisteem is ontwerp en gebou, omdat daar besluit is om die kristal deur middel van diffusie meganismes te doteer. Dié sisteem is suksesvol met die uitgloeiing van monsters by hoë temperature vir lang tydperke, in nie korrosiewe atmosfere. n' Sekondêre studie is gedoen op die migrasie van korrelgrense in polikristallyne Cu, omdat daar kommer onstaan

het dat die korrelgrens die segregasie kan beïnvloed. Hierdie studies het gewys dat die byvoeging van lae konsentrasies Sb tot polikristallyne Cu die mobiliteit van korrelgrense inhibeer.

Die veranderings in die konsentrasie op beide die oppervlakoriëntasies was gemonitor terwyl die kristal se temperatuur lineêr verhoog is teen verskillende tempo's. Die eksperimentele data is met die verbeterde Darken Model gepas. Die onttrekte Sb segregasie parameters in die Cu(110) oppervlak is: $D_0 = 2.2 \times 10^{-5}(\pm 5\%)$ m^2.s^{-1}, $Q = 196 \pm 2$ kJ.mol^{-1}, $\Delta G = -90 \pm 1$ kJ.mol^{-1} en $\Omega_{CuSb} = -5 \pm 1$ kJ.mol^{-1}, en in die Cu(111) oppervlak is dit: $D_0 = 1.1 \times 10^{-3}(\pm 5\%)$ m^2.s^{-1}, $Q = 233 \pm 2$ kJ.mol^{-1}, $\Delta G = -89 \pm 1$ kJ.mol^{-1} en $\Omega_{CuSb} = -3 \pm 1$ kJ.mol^{-1}.

Met die eksperimentele kondisies konstant, vir beide oppervlakoriëntasies, is dit gevind dat daar 'n definitiewe verandering in die pre-eksponensiële faktor en die aktiverings energie is, wat vergelykbaar is met waardes in die literatuur. Die verskil in die pre-eksponensiële faktor bied die geleentheid om die verskil in die verandering in die entropie ($\Delta S_{\Delta s}$), vir die eerste keer, te bereken vir die twee oppervlakoriëntasies as 36 J.mol^{-1}K^{-1}.

'n Uniek ontwerpte uitgloeisisteem en eksperimentele metode is suksesvol in hierdie studie gebruik, om die verskil in die Sb segregasie parameters as 'n funksie van oppervlakoriëntasie, te bevestig.

Contents

Results from this Study Already Announced   **111**

Conference Contributions   **111**

Appendix   **113**

A. Influence of Sb Doping on Grain Growth of Polycrystalline Cu   **114**

REFERENCES   **121**

Chapter 1

Introduction

Materials have to support loads, to insulate or conduct heat and electricity, to accept or reject magnetic flux, to transmit or reflect light, to survive in often hostile surroundings, and to do all this without damage to the environment or being too expensive [1 – 10].

Today surface segregation investigations have been applied in many of these aspects, for example, the study of brittle fractures [11]; grain boundary diffusion and motion [12 – 17]; the environmental effects such as integranular corrosion and stress corrosion cracking [18, 19]; especially in the catalytic field [20 – 22]. The need to develop improved catalysts for use in connection with environmental protection and the creation of viable alternative energy systems have led to an increasing use of metal alloys as heterogeneous catalysts, in which surface concentration plays a key role in controlling such important factors as activity and selectivity.

Surface segregation has, within the past 20 years, become a very active area of research with both fundamental and practical research goals.

From literature [23] it is said that, the most basic definition of segregation may be expressed as 'the redistribution of solute atoms between the surface and bulk of a crystal such that the total energy of the crystal is minimised'. Two of the reasons why the total energy of a crystal reduces, during segregation, are the reduction of the deformation tension in the crystal and the surface energy [24].

Impurity atoms that are distributed in a crystal and that are bigger than the crystal atoms will cause the crystal lattice to deform. This deformation of the crystal lattice increases the

tension (energy) in the crystal. These impurity atoms distributed in the crystal will then segregate to the surface minimizing the tension of the crystal lattice and therefore reducing the total energy of the crystal [25, 26].

The atom with the least amount of surface energy will segregate to the surface reducing the energy in the crystal. The surface energy is seen as the energy per unit area that is needed to form a new surface by breaking bonds.

1.1. The Objectives of this Study

Terblans [27] compiled a theoretical model that indicates that the surface orientation of a crystal influences the bulk diffusion coefficient. There have been attempts [27 – 30] to measure this, but there were many variables due to the fact that different single crystals (different surface orientations) was used and were not measured at the same conditions.

- The purpose of this study, therefore, is to confirm this theory by obtaining experimental Sb segregation parameters from a Cu crystal with two different surface orientations (a bi-crystal) separated by a grain boundary, thus keeping most variables the same for the two orientations.

- In order to measure the segregation in both surfaces at the same conditions the AES system had to be modified so that the e^- beam can be deflected from surface to surface while the temperature of the crystal is ramped linearly.

- This study lead to the development of an annealing system, able to anneal samples at relatively high temperatures for long periods of time in an inert gas atmosphere.

- Because a bi-crystal was used, a secondary study on the migration of the grain boundary under certain conditions was unavoidable.

1.2. The Outline

Chapter 2 starts with the theory of segregation by discussing some diffusion mechanisms. A brief history on how diffusion research started as well as the kinetics of segregation and equilibrium segregation are discussed. The chapter concludes with an overview of the Modified Darken Model that describes both the kinetic as well as the equilibrium segregation process.

In **chapter 3** the theory of how the surface orientation of a crystal influences the bulk diffusion coefficient is discussed. The relation between the vacancy formation energy and the surface orientation is shown.

In **chapter 4** a newly designed and built annealing system that can be filled with Ar gas to high gauge pressures is presented. Discussed in this chapter are the mechanical setup and the electronic control unit of the system. XPS results are also presented confirming the successful operation of the system. A proposed annealing procedure, used in this investigation, is described in detail.

In **chapter 5,** the experimental setup is given. The dimensions of the bi-crystal, sample preparation, apparatus and experimental procedures are discussed. The modifications of the AES system and the computer program for controlling the AES spectrometer are also discussed.

Chapter 6 presents the experimental results obtained from the bi-crystal doped with Sb. In this chapter the procedure that was used to fit the experimental data with the Modified Darken Model is also discussed.

In **chapter 7** the results are discussed showing the difference in the segregation parameters from the two different surfaces. This difference is compared to the theoretical difference.

The difference in the change in entropy is also calculated in this chapter. This chapter concludes by comparing the results obtained from this study with other published results indicating the success of the study.

Chapter 2

Diffusion Mechanisms and Segregation Theory

2.1   Diffusion Mechanisms

Any theory of atom diffusion in solids should start with a discussion of diffusion mechanisms. One should answer the question: 'How does this particular atom move from here to there?' In crystalline solids, it is possible to describe diffusion mechanisms in simple terms. The crystal lattice restricts the positions and the migration paths of atoms and allows a simple description of each specific atom's displacement.

The diffusion coefficient in general, is determined on both the jump frequency and the jump distance. Both these dependents are properties determined by the material.

The diffusion coefficient is also determined by the type of mechanism that an atom uses to move through the crystal. The ease of movement of this atom through the crystal is influenced by factors like the relative size of the diffusing atom and whether the diffusion is mediated by defects or not.

Some of the most important diffusion mechanisms that are found in metals are interstitial mechanism, ring mechanism and the vacancy mechanism [31].

2.1.1 Interstitial Mechanism

Solute atoms that are considerably smaller then the matrix atoms are incorporated in interstitial sites of the host lattice, thus forming an interstitial solid solution. In fcc and bcc lattices interstitial solutes occupy octahedral and or tetrahedral interstitial sites as indicated in the figure below.
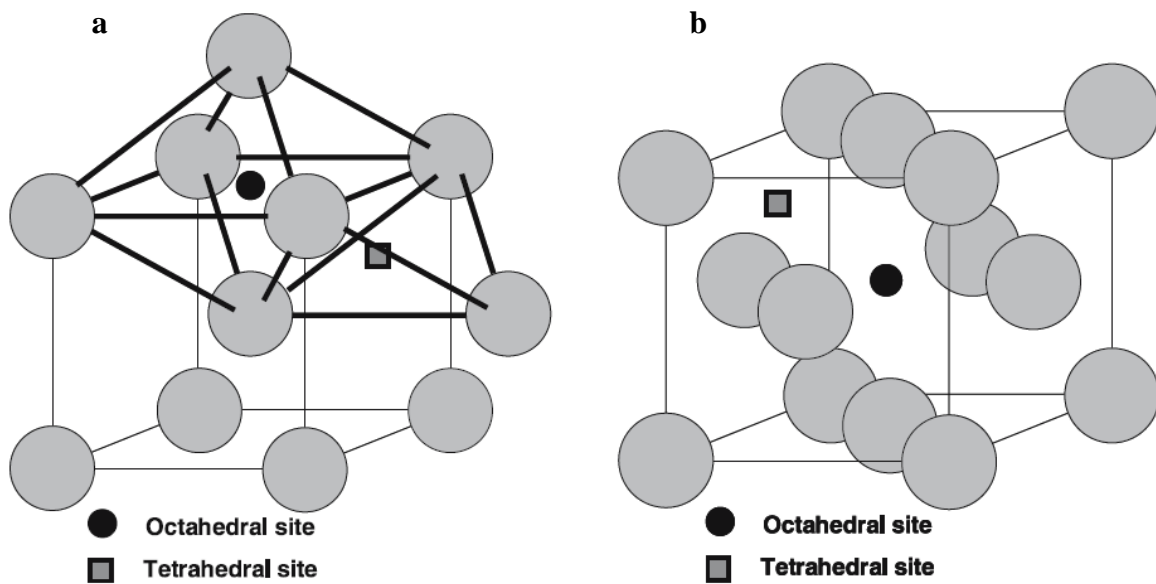
Figure 2.1: Octahedral and tetrahedral interstitial sites in the bcc (a) and fcc (b) lattice.

An interstitial solute can diffuse by jumping from one interstitial site to one of its neighbouring sites as shown below (see **figure 2.2**). The solute is thus diffusing by an interstitial mechanism.
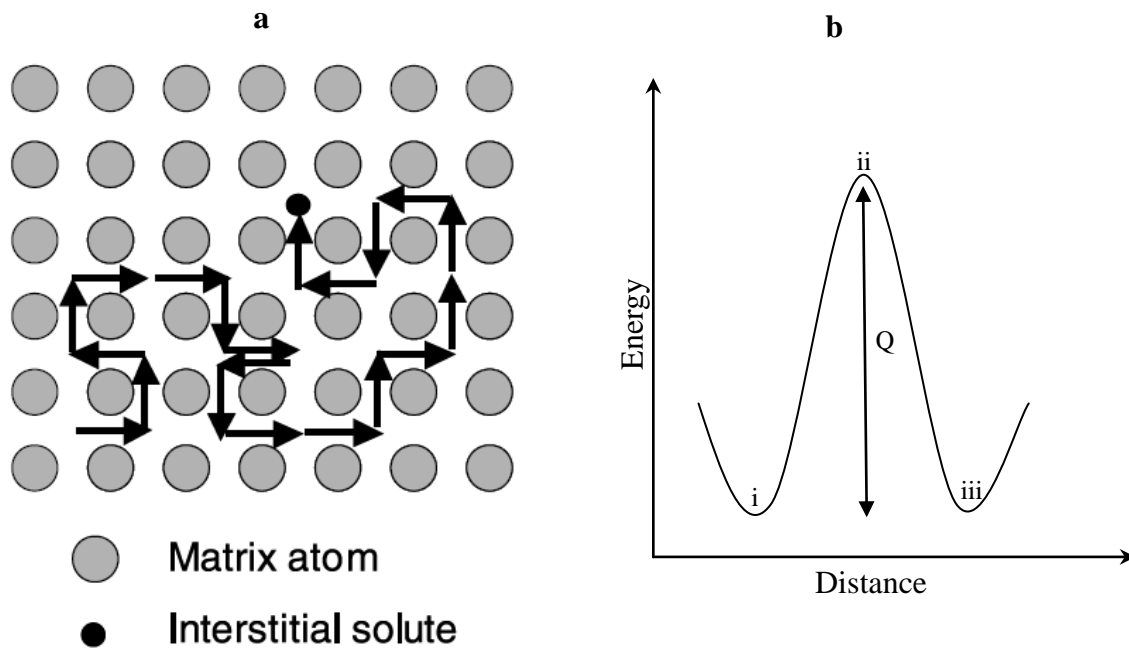
Figure 2.2: Direct interstitial mechanism of diffusion (a) and the saddle point configuration (b).

Consider the atomic movements during a jump as depicted in **figure 2.2 (a, b)**, the interstitial starts from an equilibrium position (i), reaches the saddle-point configuration (ii) where maximum lattice straining occurs, and settles again on an adjacent interstitial site (iii). In the saddle-point configuration neighbouring matrix atoms must move aside to let the solute atom through. When the jump is completed, no permanent displacement of the matrix atoms remains. Conceptually, this is the simplest diffusion mechanism. It is also denoted as the direct interstitial mechanism.

This mechanism is relevant for diffusion of small impurity atoms such as H, C, N, and O in metals and other materials. Small atoms fit in interstitial sites and in jumping do not greatly displace the matrix atoms from their normal lattice sites [31].

2.1.2 Ring Mechanism

Solute atoms similar in size to the matrix atoms usually form substitutional solid solutions. The diffusion of substitutional solutes and of matrix atoms themselves requires a mechanism different from interstitial diffusion.

In the 1930's it was suggested that self- and substitutional solute diffusion in metals occurs by a direct exchange of neighbouring atoms, in which two atoms move simultaneously. In a close-packed lattice this mechanism requires large distortions to squeeze the atoms through. This entails a high activation barrier and makes this process energetically unfavourable.
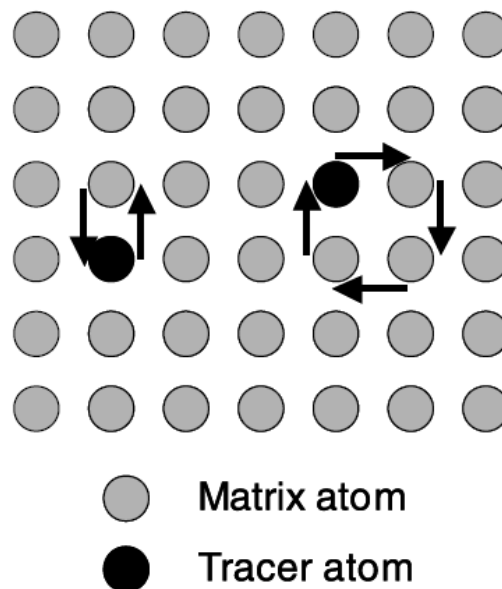
Figure 2.3: Direct exchange and ring diffusion mechanism.

Theoretical calculations for self-diffusion of Cu performed by Huntington et al. in the 1940's, which were later confirmed by more sophisticated theoretical approaches, led to the conclusion that direct exchange, at least in close-packed structures, was not a likely mechanism.

The so called ring mechanism of diffusion was proposed for crystalline solids in the 1920's by the American metallurgist, Jeffries, and advocated by Zener in the 1950's. The ring mechanism corresponds to a rotation of 3 (or more) atoms as a group by one atom distance (see **figure 2.3**). The required lattice distortions are not as great as in a direct exchange. Ring versions of atomic exchanges have lower activation energies but the probability of three or more atoms moving at the same time is minuscule, which makes this more complex mechanism unlikely for most crystalline substances.

2.1.3   Vacancy Mechanism

As knowledge about solids expanded, vacancies have been accepted as the most important form of thermally induced atomic defects in metals. It has also been recognised that the dominant mechanism for the diffusion of matrix atoms and of substitutional solutes in metals is the vacancy mechanism. An atom is said to diffuse by this mechanism, when it jumps into a neighbouring vacancy.
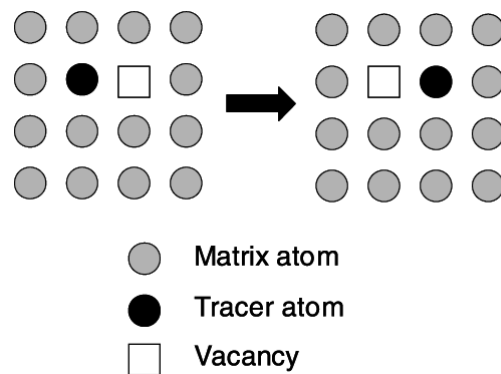
Figure 2.4: Vacancy mechanism of diffusion.

The constriction, which inhibits motion of an adjacent atom into a vacancy in a close-packed lattice, is small as compared to the constriction against the direct interstitial or ring exchange. Each atom moves through the crystal by making a series of exchanges with vacancies, which from time to time are in its vicinity. The number of vacancies in a monoatomic crystal, at a temperature T, can be determined by [27]:

$$N_v = N_0 \exp\left(\frac{-E_v}{RT}\right) \tag{2.1}$$

where N_0 is the number of lattice sites, E_v the vacancy formation energy and R the universal gas constant.

The vacancy mechanism is the dominating mechanism of self-diffusion in metals and substitutional alloys.

In the next paragraph the segregation kinetics and segregation equilibrium will be discussed.

2.2 Segregation

Robert Boyle (1627-1691) was, according to reference [32], the first author of an experimental demonstration of solid state diffusion. He observed the penetration of a "*solid heavy body*" in a farthing (a small copper coin), so that this side took on a golden colour, while the other side kept its original one. He explained in his essay [32]: "*To convince the scrupulous, that the pigment really did sink... and did not merely colour the superficies,... By filing off a wide gap from the edge of the coin towards, it plainly appeared that the golden colour had penetrated a pretty way beneath the surface of the farthing.*" Boyle successfully synthesized brass by means of inter-diffusion.

The first systematic diffusion study was due to a Scottish Chemist, Thomas Graham, born in 1805 in Glasgow. He was the inventor of dialysis, and was considered as the leading chemist of his generation [33]. The first lines of his paper on systematic diffusion, published in the Philosophical Magazine in 1833 [34] read as follow: "*Fruitful as the miscibility of the gases has been in interesting speculations, the experimental information we possess on the subject amounts to little more than the well established fact, that gases of different nature, when brought into contact, do not arrange themselves according to their density, the heaviest under most, and the lighter uppermost, but they spontaneously diffuse, mutually and equally, through each other, and so remain in the intimate state of mixture for any length of time.*"

After which Adolf Fick, who was a leading- and today a famous physiologist, proposed the first quantitative laws of diffusion. By commenting on the paper of Thomas Graham, he wrote in a paper published in 1855, in the Philosophical Magazine [35]: "*A few years ago, Graham published an extensive investigation on the diffusion of salts in water, in which he more especially compared the diffusibility of different salts. It appears to me a matter of regret, however, that in such an exceedingly valuable and extensive investigation, the development of a fundamental law, for the operation of diffusion in a single element of space, was neglected, and I have therefore endeavoured to supply this omission.*"

At this time, diffusion measurements by Graham and Fick were confined to fluids as these measurements were possible at temperatures around room temperature. In the second part of the nineteenth century, metallurgical studies on materials opened the way to the study of diffusion in metals. Quantitative measurements were only performed before the very last years of the nineteenth century by the famous metallurgist William Chandler Roberts-Austen, who worked as an assistant for Thomas Graham. He is known for his study of the equilibrium diagram Fe-C. The excellent micrographs, due to his French friend Floris

Osmond, of specimens of carburised iron, clearly showed the penetration of C inside the bulk of Fe. Roberts-Austin used the Arrhenius graph, proposed by Svante Arrhenius in his 1889 paper [36], to extract coefficients of diffusion which are comparable to modern values [37].

In 1905 Albert Einstein derived the fundamental relation between a macroscopic quantity (i.e. coefficient of diffusion) and a microscopic one (the mean square displacement) [38].

Fick's laws proved successful in various areas; but with the arrival of techniques capable of measuring concentration gradients in solids, it became evident that the data usually diverged from these predictions. Therefore, in 1942, Darken proposed that diffusion might depend on the gradient of the 'effective' concentration, i.e. of the activity, rather than of the actual concentration as such [39]. Darken's approach is macroscopic and based on thermodynamics, thus it could be seen as an attractive model for industrial types of research. The Darken model is not one hundred percent correct, as is with most theoretical models, but research on "perfecting" diffusion models is done daily.

2.2.1 Segregation Kinetics

Segregation kinetics can be defined as the rate at which impurity atoms diffuse from the bulk to the surface of a crystal. Impurity atoms from the bulk of the crystal, where the impurity concentration is relatively large, diffuse to the surface of the crystal where the concentration is relatively low. This is contradictory to the Fick Model because according to Fick, diffusion is a concentration driven process.

According to the Fick Model it is assumed that the impurity concentration is initially homogeneous. Mathematically it can be written as:

$$C^x = C^b \quad \text{for} \quad x > 0 \quad \text{and} \quad t = 0$$

It can be seen that, as soon as the atoms segregate to the surface they are removed, thus keeping the surface concentration zero. This is written mathematically as:

$$C^x = 0 \quad \text{for} \quad x = 0 \quad \text{and} \quad t \geq 0$$

These conditions are used to solve Fick's first law by means of Laplace transformations.

$$\frac{\partial C}{\partial t} = D \frac{\partial^2 C}{\partial x^2} \tag{2.2}$$

This is described in the book of Crank: "The Mathematics of Diffusion" [40]. The solution to Fick's first law, which describes the bulk concentration, is given by the following equation:

$$C^x = C^{x_0} \operatorname{erf}\left(\frac{x}{2\sqrt{Dt}}\right) \tag{2.3}$$

where C^x is the bulk concentration at a distance x, in the bulk, after a time t, C^{x_0} the initial bulk concentration and D the diffusion coefficient.

Equation 2.3 can then be used to derive an expression for the flux of atoms trough an area A at $x = 0$.

$$J_{x=0} = \left(D\frac{\partial C}{\partial x}\right)_{x=0} = \frac{DC^{x_0}}{\sqrt{\pi Dt}} \tag{2.4}$$

With a known flux, J, at distance $x = 0$, the total amount of atoms, M_t, that moves through the area A at $x = 0$ in the time $t = t_1$ can be calculated by integrating the flux.

$$M_t = A \int_0^{t_1} J dt \tag{2.5}$$

$$M_t = 2AC^{x_0}\left(\frac{Dt}{\pi}\right)^{\frac{1}{2}} \tag{2.6}$$

It is then assumed that atoms moving through the plane go and sit in the surface layer. Thus the concentration of the diffusing atoms in the surface layer can be calculated by taking the

total amount of atoms in the surface layer and dividing the volume of this surface layer, resulting in **equation 2.7**:

$$C^{\emptyset} = \frac{\left[2AC^{x_0}\left(\frac{Dt}{\pi}\right)^{\frac{1}{2}}\right]}{Ad} \tag{2.7}$$

where d is the inter atomic distance.

Fulfilling the condition that the initial impurity bulk concentration (C^{x_0}) is homogeneous, C^{x_0} must be added to **equation 2.7** resulting in:

$$C^{\emptyset} = C^{x_0}\left[1 + \frac{2}{d}\left(\frac{Dt}{\pi}\right)^{\frac{1}{2}}\right] \tag{2.8}$$

where $C^{\emptyset}$ is the surface concentration and C^{x_0} the initial bulk concentration.

This equation is well known as Fick's second law and is commonly used to calculate the surface concentration in segregation studies. This equation's biggest drawbacks could be that it can only describe the kinetics of segregation and that it perceives the diffusion process as a concentration driven process, but in fact the process is not concentration driven as the impurity atoms move from an area where the concentration is low to an area where it is high and thus violating the concentration driven process.

During the segregation process, with increasing temperature, the kinetic part will stop as the equilibrium part of segregation will start.

2.2.2   Segregation Equilibrium

To be able to derive an expression for equilibrium segregation it is necessary to extend the basic definition (see **chapter 1**):

i. The crystal is regarded as a closed system consisting of two phases, surface ($\emptyset$) and bulk (B) which are both open systems.

ii. The surface is considered to be finite with a finite number of atoms ($n^\emptyset = constant$) and the bulk infinite in size with infinite number of atoms ($n^B = \infty$).

iii. Atoms are exchanged between the two phases until the total energy of the crystal is at a minimum. Thus the conservation of atoms requires that $\delta n_i^\emptyset = -\delta n_i^B$.

The equilibrium condition for a closed system consisting of p phases can be described in terms of the change in the total energy of the crystal by [41]:

$$(\delta E)_{S,V,n_i} = \sum_{v=1}^{p} \delta E^v \geq 0 \qquad (2.9)$$

The term δE can be expanded as:

$$\delta E^v = T^v \delta S - P^v \delta V^v + \delta G^v \qquad (2.10)$$

where T^v is the temperature, δS^v the change in entropy, P^v the pressure, δV^v the volume change and δG^v the change in the Gibbs free energy of phase v. If the temperature and pressure is the same for all the phases (as in the case for this study), it may be shown that **equation 2.10** reduces to:

$$(\delta E)_{n_i} = (\delta G)_{n_i} \geq 0 \qquad (2.11)$$

According to **equation 2.11** the change in the Gibbs free energy can be used to describe the equilibrium condition (the minimum energy condition) of the crystal. The advantage of this formulation is that the Gibbs free energy (G) can be expanded in terms of the chemical potentials (μ) of the various constituents and that the equilibrium condition may be expressed as a function of the chemical potential terms as shown below:

$$G^v = \sum_{i=1}^{m} n_i^v \mu_i^v \qquad (2.12)$$

where n_i^γ is the number of moles of atoms i to m in phase ν and μ_i^γ the chemical potential of atoms i in phase ν.

Therefore the total Gibbs free energy of the crystal containing two phases (bulk (B) and surface (Ø)) is given by equations below:

$$G_{Total} = \sum_{i=1}^{p} G^\nu = \sum_{\nu=1}^{p} \sum_{i=1}^{m} (n_i^\gamma \mu_i^\gamma) \tag{2.13}$$

$$G_{Total} = G^\emptyset + G^B \tag{2.14}$$

$$G_{Total} = \sum_{i=1}^{m} n_i^\emptyset \mu_i^\emptyset + \sum_{i=1}^{m} n_i^B \mu_i^B \tag{2.15}$$

The variation in the Gibbs free energy is thus:

$$\delta G = \sum_{\nu=1}^{p} \left[\left(\sum_{i=1}^{m} (\delta n_i^\gamma \mu_i^\gamma) \right) + \left(\sum_{i=1}^{m} (n_i^\gamma \delta \mu_i^\gamma) \right) \right] \tag{2.16}$$

$$\delta G = \left[\left(\sum_{i=1}^{m} (\delta n_i^\emptyset \mu_i^\emptyset) \right) + \left(\sum_{i=1}^{m} (\delta n_i^B \mu_i^B) \right) \right] + \left[\left(\sum_{i=1}^{m} (n_i^\emptyset \delta \mu_i^\emptyset) \right) + \left(\sum_{i=1}^{m} (n_i^B \delta \mu_i^B) \right) \right] \tag{2.17}$$

The equilibrium condition of a closed system can thus be described in terms of the chemical potential as:

$$\sum_{\nu=1}^{p} \left[\sum_{i=1}^{m} (\delta n_i^\gamma \mu_i^\gamma) + \sum_{i=1}^{m} (n_i^\gamma \delta \mu_i^\gamma) \right] \geq 0 \tag{2.18}$$

The second term in **equation 2.17** is the well known Gibbs-Duhem relation that is equal to zero [41]. **Equation 2.17** thus reduces to:

$$\delta G = \left[\sum_{i=1}^{m} (\delta n_i^\emptyset \mu_i^\emptyset) + \sum_{i=1}^{m} (\delta n_i^B \mu_i^B) \right] \tag{2.19}$$

From the extended basic definition of segregation above (ii), the phase Ø (surface) has a limited volume and can thus only accommodate $n^\emptyset$ atoms in the surface. This is:

$$\sum_{i=1}^{m} n_i^\emptyset = n^\emptyset \tag{2.20}$$

Furthermore, from the extended basic definition above (iii), if the atoms are exchanged between the phases $\emptyset$ and B, the conservation of atoms requires that:

$$\delta n_i^{\emptyset} = -\delta n_i^{B} \tag{2.21}$$

Also, as stated in the extended definition (ii), the amount of atoms in the surface stay constant meaning that for every atom jumping out of the surface there is another jumping in the surface. Thus the sum of the change in the amount of atoms in the surface is zero.

$$\delta n_1^{\emptyset} + \delta n_2^{\emptyset} + \cdots + \delta n_m^{\emptyset} = 0 \tag{2.22}$$

Equation 2.22 can be rewritten making the mth term the subject of the equation:

$$-\delta n_m^{\emptyset} = \delta n_1^{\emptyset} + \delta n_2^{\emptyset} + \cdots + \delta n_{m-1}^{\emptyset} \tag{2.23}$$

By substituting **equation 2.23** into **equation 2.19** with a few manipulations it is possible to describe the change in the Gibbs free energy as:

$$= \left[\sum_{i=1}^{m-1} \left(\mu_i^{\emptyset} - \mu_i^{B} - \mu_m^{\emptyset} + \mu_m^{B} \right) \delta n_i^{\emptyset} \right] \geq 0 \tag{2.25}$$

Because the $(m-1)$ $\delta n_i^{\emptyset}$'s are independent the only way in which **equation 2.25** can be satisfied is if:

$$\left(\mu_i^{\emptyset} - \mu_i^{B} - \mu_m^{\emptyset} + \mu_m^{B} \right) = 0 \tag{2.26}$$

Equation 2.26 is thus the equilibrium condition in terms of the chemical potential [23].

For a binary alloy, the equilibrium condition can be described by rewriting **equation 2.26**:

$$\mu_1^{\emptyset} - \mu_1^{B} - \mu_2^{\emptyset} + \mu_2^{B} = 0 \tag{2.27}$$

According to the regular solution model, developed by Hildebrand [42], the chemical potential of atoms in a binary alloy can be described in terms of the concentration, standard chemical potential and the interaction parameter:

$$\mu_1^\nu = \mu_1^{0,\nu} + \Omega_{12}(X_2^\nu)^2 + RTln(X_1^\nu)$$

$$\mu_2^\nu = \mu_2^{0,\nu} + \Omega_{12}(X_1^\nu)^2 + RTln(X_2^\nu)$$

(2.28)

where μ_1^ν is the chemical potential of the matrix atoms (Cu atoms) in phase ν, $\mu_1^{0,\nu}$ the standard chemical potential of the matrix atoms in phase ν, Ω_{12} the chemical interaction parameter between the matrix and the impurity atoms, X_2^ν the concentration of the impurity atoms in phase ν, R the universal gas constant, X_1^ν the concentration of the matrix atoms in phase ν, μ_2^ν is the chemical potential of the impurity atoms in phase ν and $\mu_2^{0,\nu}$ the standard chemical potential of the impurity atoms in phase ν.

This model is based on three assumptions:

i. Atoms are randomly distributed over positions in a three dimensional lattice

ii. No vacancies exist

iii. The energy of the system may be expressed as the sum of pair wise interaction between neighbouring atoms

Using **equation 2.28** it is possible to then describe the chemical potential of the different atoms in the bulk and surface as follow:

$$\mu_1^{\emptyset} = \mu_1^{0,\emptyset} + \Omega_{12}\left(X_2^{\emptyset}\right)^2 + RTln\left(X_1^{\emptyset}\right)$$

$$\mu_2^{\emptyset} = \mu_2^{0,\emptyset} + \Omega_{12}\left(X_1^{\emptyset}\right)^2 + RTln\left(X_2^{\emptyset}\right)$$

$$\mu_1^{B} = \mu_1^{0,B} + \Omega_{12}(X_2^{B})^2 + RTln(X_1^{B})$$

$$\mu_2^{B} = \mu_2^{0,B} + \Omega_{12}(X_1^{B})^2 + RTln(X_2^{B})$$

(2.29)

When **equation 2.27** is therefore expanded in terms of the regular solution model, the Bragg-Williams equilibrium segregation equation is obtained:

$$\frac{X_1^{\emptyset}}{1-X_1^{\emptyset}} = \frac{X_1^{B}}{1-X_1^{B}}exp\left[\frac{\Delta G + 2\Omega_{12}\left(X_1^{\emptyset}-X_1^{B}\right)}{RT}\right] \qquad (2.30)$$

where $X_1^{\emptyset}$ is the surface concentration of the impurity, X_1^{B} the bulk concentration of the impurity and $\Delta G = \mu_1^{0,B} - \mu_1^{0,\emptyset} - \mu_2^{0,B} + \mu_2^{0,\emptyset}$ the segregation energy.

By setting the interaction parameter equals to zero in equation **2.30** the Bragg-Williams equation reduces in the simpler well known Langmuir-McLean equation:

$$\frac{X_1^{\emptyset}}{1-X_1^{\emptyset}} = \frac{X_1^{B}}{1-X_1^{B}}exp\left(\frac{\Delta G}{RT}\right) \qquad (2.31)$$

Combining the Fick model and the Bragg-Williams equations, however, do not completely describe the segregation process. The all-embracing model that describes both the kinetic as well as the equilibrium segregation process adequately is the Modified Darken Model.

2.2.3   The Modified Darken Model

The Darken model considers the difference in the chemical potential energy between the multi-layers as the driving force behind segregation [23, 39, 43]. Impurity atoms will diffuse from the bulk, an area with a high chemical potential, to the surface, an area with a low chemical potential.

This model was first developed by Darken in 1949 [39] and proposed that the net flux of impurity atoms (i) through a plane at $x = b$ be described in terms of the chemical potential as follow:

$$J_i = -M_i X_i^B \left(\frac{\partial \mu_i}{\partial x} \right)_{x=b} \tag{2.32}$$

where M_i is the mobility of the specified atoms (i), X_i^B the bulk (supply) concentration of the specified atoms (i) in the plane and μ_i the chemical potential of the specified atoms (i).

The big difference between the Fick and Darken model is the driving force that makes diffusion takes place. According to the Fick model, the diffusion driving force is the concentration gradient. Darken sees the diffusion driving force as the minimization of the total energy of the crystal.

Du Plessis [23] modified the original Darken Model to give a more physically correct description of the model. The modifications are as follow:

1. The crystal is seen as $N + 1$ discrete stacked up layers, of thickness d, parallel to the surface. The thickness d of the layers is the same as the inter-atomic distance.

2. The term $\left(\frac{\partial \mu_i}{\partial x} \right)$ for the change in chemical potential (μ_i) with distance (x) is written in a discrete form:

$$-\frac{\partial \mu_i}{\partial x} = \frac{\Delta \mu^{(j+1 \rightarrow j)}}{d} \tag{2.33}$$

3. The change in chemical potential is written as:

$$\Delta \mu_i^{(j+1 \rightarrow j)} = \left(\mu_i^{(j+1)} - \mu_i^{(j)} \right) - \left(\mu_m^{(j+1)} - \mu_m^{(j)} \right) \qquad (2.34)$$

where $\mu_i^{(j+1)}$ is the chemical potential of the impurity atoms in the $(j+1)^{\text{th}}$ layer, $\mu_i^{(j)}$ the chemical potential of the impurity atoms in the $(j)^{\text{th}}$ layer, $\mu_m^{(j+1)}$ is the chemical potential of the matrix atoms in the $(j+1)^{\text{th}}$ layer and $\mu_m^{(j)}$ is the chemical potential of the matrix atoms in the $(j)^{\text{th}}$ layer.

4. The concentration of the impurity atoms C_i^b that is defined in the original Darken Model as the supply concentration in between two layers (within the plane at $x = b$) has got no physical meaning. Du Plessis [23] suggested that the concentration of the layer from which the atoms diffuse determines the flux of the atoms to the next layer as it is seen as the supplier of the atoms.

$$J_i^{(j+1 \rightarrow j)} = M_i C_i^{(j+1)} \frac{\Delta \mu^{(j+1 \rightarrow j)}}{d} \qquad (2.35)$$

Equation 2.35 thus indicates the flux of atoms from the $(j+1)^{\text{th}}$ layer to the $(j)^{\text{th}}$ layer with $C_i^{(j+1)}$ as the supply concentration.

If $\Delta \mu_i^{(j+1 \rightarrow j)} > 0$ it means that there is a decrease in the Gibbs free energy as the impurity atoms diffuse from the $(j+1)^{\text{th}}$ layer to the $(j)^{\text{th}}$ layer and thus making $C_i^{(j+1)}$ the supply concentration. Thus when $\Delta \mu_i^{(j+1 \rightarrow j)} < 0$ it means that there is a decrease in the Gibbs free energy as the impurity atoms diffuse from the $(j)^{\text{th}}$ layer to the $(j+1)^{\text{th}}$ layer making $C_i^{(j)}$ the supply concentration. Mathematically it can be written as follow:

$$J_i^{(j+1 \rightarrow j)} = M_i C_i^{(j+1)} \left| \frac{\Delta \mu^{(j+1 \rightarrow j)}}{d} \right| \quad if \quad \Delta \mu_i^{(j+1 \rightarrow j)} > 0 \qquad (2.36)$$

$$J_i^{(j\to j+1)} = M_i C_i^{(j)} \left| \frac{\Delta\mu^{(j\to j+1)}}{d} \right| \quad if \quad \Delta\mu_i^{(j+1\to j)} < 0 \tag{2.37}$$

The rate at which the impurity concentration in the $(j)^{th}$ layer changes, can be calculated with the help of the flux **equations 2.36** and **2.37.**

$$\frac{\partial c_i^{(j)}}{\partial t} = \frac{\left(J_i^{(j+1\to j)} - J_i^{(j\to j-1)}\right)}{d} \tag{2.38}$$

Equation 2.38 can be expanded to a set of $(m-1)(N+1)$ rate equations with which the rate of the impurity atoms' concentration increases in the $(j)^{th}$ layer can be calculated.

$$\frac{\partial X_i^{\emptyset}}{\partial t} = \left(\frac{M_i^{(B_1\to\emptyset)} X_i^{B_1}}{d^2} \Delta\mu_i^{(B_1\to\emptyset)} \right)$$

$$\frac{\partial X_i^{B_1}}{\partial t} = \left(\frac{M_i^{(B)} X_i^{B_2}}{d^2} \Delta\mu_i^{(B_2\to B_1)} - \frac{M_i^{(B_1\to\emptyset)} X_i^{B_1}}{d^2} \Delta\mu_i^{(B_1\to\emptyset)} \right)$$

$$.$$
$$.$$
$$.$$

$$\frac{\partial X_i^{j}}{\partial t} = \left(\frac{M_i^{(B)} X_i^{(j+1)}}{d^2} \Delta\mu_i^{(j+1\to j)} - \frac{M_i^{(B)} X_i^{j}}{d^2} \Delta\mu_i^{(j\to j-1)} \right)$$

$$.$$
$$.$$
$$.$$

$$\tag{2.39}$$

for $i = 1,2,\ldots,m-1$ and $j = \emptyset, B_1, B_2, \ldots, B_{N+1}$

This set of differential equations can be solved numerically as is discussed by Terblans [27]. The solution to this set of equations makes it possible to calculate the concentration of the impurity atoms in any layer as a function of time.

For a binary alloy elemental composition $m = 2$, which implies that $i = 1$, is the solute in the alloy. The rate equations are as follow:

34

$$\frac{\partial X_1^{\emptyset}}{\partial t} = \left(\frac{M_1^{(B_1 \to \emptyset)} X_1^{B_1}}{d^2}\right)\left[\Delta G + RT\ln\frac{X_1^{B_1}\left(1-X_1^{\emptyset}\right)}{X_1^{\emptyset}\left(1-X_1^{B_1}\right)} + 2\Omega_{12}\left(X_1^{\emptyset} - X_1^{B_1}\right)\right]$$

$$\frac{\partial X_1^{B_1}}{\partial t} = \left(\frac{M_1^{B} X_1^{B_2}}{d^2}\right)\left[RT\ln\frac{X_1^{B_2}\left(1-X_1^{B_1}\right)}{X_1^{B_1}\left(1-X_1^{B_2}\right)} + 2\Omega_{12}\left(X_1^{B_1} - X_1^{B_2}\right) - RT\ln\frac{X_1^{B_1}\left(1-X_1^{\emptyset}\right)}{X_1^{\emptyset}\left(1-X_1^{B_1}\right)} - 2\Omega_{12}\left(X_1^{\emptyset} - X_1^{B_1}\right)\right]$$

$$\vdots$$

$$\frac{\partial X_1^{BN}}{\partial t} = \left(\frac{M_1^{B} X_1^{BN+1}}{d^2}\right)\left[RT\ln\frac{X_1^{BN+1}\left(1-X_1^{BN}\right)}{X_1^{BN}\left(1-X_1^{BN+1}\right)} + 2\Omega_{12}\left(X_1^{BN} - X_1^{BN+1}\right) - RT\ln\frac{X_1^{BN}\left(1-X_1^{BN-1}\right)}{X_1^{N-1}\left(1-X_1^{BN}\right)} - 2\Omega_{12}\left(X_1^{N-1} - X_1^{BN}\right)\right]$$

$$\vdots$$

$$(2.40)$$

During the derivation of the above equations it is assumed that the binary solution is an ideal solution and therefore the following assumption must be true:

$$X_1^{j} + X_2^{j} = 1 \tag{2.41}$$

where X_1^{j} is the fractional concentration of the impurity atoms in the jth layer and X_2^{j} the fractional concentration of the matrix atoms in the same layer (j^{th} layer).

This set of rate equations (**equation 2.40**) is able to describe the kinetics as well as the equilibrium part of segregation.

In this Darken model the term mobility (M) is used. This term is similar to the diffusion coefficient (D), also used in the Fick model. As this term of the diffusion coefficient is already well established, Darken wrote the mobility in terms of the diffusion coefficient [39].

$$M = \frac{D}{RT} \tag{2.42}$$

This can actually only be done for an ideal solution and is thus valid and correct for a very dilute solution, which could be seen as an ideal solution.

Chapter 3

Segregation and Vacancy Diffusion

3.1   Introduction

Does the surface orientation of a crystal influence the bulk diffusion coefficient? In this chapter the relation between the vacancy formation energy and the surface orientation will be discussed. The diffusion coefficient will then be derived and from that it will be indicated that the surface orientation influences the bulk diffusion coefficient.
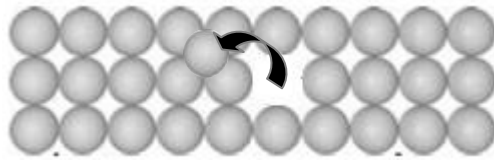
3.2   The Forming of Vacancies in a Crystal

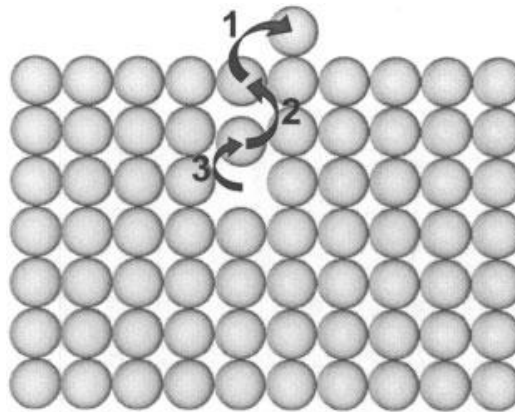
Figure 3.1: The Frenkel defect mechanism.

Figure 3.2: The Schottky defect mechanism.

There are two types of mechanisms whereby a vacancy in a crystal can form [44 – 46]. The first mechanism is the so called Frenkel defect mechanism. According to this mechanism a vacancy is formed in the crystal through an atom that jumps out of its lattice position and sits in an interstitial position as depicted in **figure 3.1**. Since the atom that sits in the interstitial position deforms the crystal lattice, the amount of energy needed to form a Frenkel defect is relatively high. A Frenkel defect is thus seldom formed in metals.

The second mechanism is the so called Schottky vacancy forming mechanism. In this event a vacancy is formed through an atom that jumps out of the surface to form an adatom as depicted in **figure 3.2**. An atom in the bulk just beneath the surface layer then jumps in the

vacancy in the surface layer. In this process the vacancy moves into the bulk and thus it can be seen, as if an atom is removed from the bulk and placed on the surface to form a vacancy in the bulk. The amount of energy needed to form a vacancy by means of this type of mechanism is much lower than that for the Frenkel mechanism. The Schottky vacancy forming mechanism is thus seen as the primary vacancy forming mechanism in a metal crystal.

Statistically it can be shown that the equilibrium fractional concentration of vacancies in a crystal can be calculated with [27, 41, 45, 46]:

$$X_v = e^{-E_v/RT} \tag{3.1}$$

where E_v is the vacancy formation energy and X_v the fractional vacancy equilibrium concentration at a temperature T.

It is assumed that vacancies are formed only by the Schottky mechanism. Vacancies are thus formed in the surface layer and diffuse down in the crystal (bulk). The surface thus acts as a supplier of vacancies. Terblans [27] showed that the vacancy forming energy can be written in terms of the chemical potential:

$$E_v = \mu_v^{0,B} - \mu_v^{0,\emptyset} \tag{3.2}$$

where $\mu_v^{0,B}$ is the standard chemical potential of a vacancy in the bulk and $\mu_v^{0,\emptyset}$ the standard chemical potential of a vacancy on top of the surface layer.

Because the chemical potential is the energy per particle, the vacancy formation energy is thus the energy needed to remove an atom from the bulk minus the energy gained when the atom is placed on the surface [27, 47, 48].

In the next section the influence of the surface orientation on the vacancy formation energy is discussed.

3.3 Vacancy Formation Energy and the Influence of Surface Orientation

If an atom is removed from the bulk, energy is needed to break the bonds of the atom. When this atom is placed on the surface of the crystal, bonds are made with the adatom and energy is released. The vacancy forming energy (E_v) is thus the net energy needed to remove an atom from the bulk and form an adatom. This energy can be calculated with the following equation:

$$E_v = E_{coh}^B - E_{coh}^{adatom} \tag{3.3}$$

where E_{coh}^B is the cohesion energy of an atom in the bulk and E_{coh}^{adatom} the cohesion energy of the adatom [27].

E_{coh}^B can be approached by simply counting the number of bonds with the atom in the bulk and multiplying that with the binding energy factor f (cohesion energy factor), where $f_{Cu} \approx -0.29$ [27, 49]. Similarly, E_{coh}^{adatom} can be calculated by counting the number of bonds with the adatom.

In a metal, an atom forms a bond with each neighbouring atom. For a fcc crystal structure the atom in the bulk has 12 neighbouring atoms and thus form 12 bonds. The cohesion energy of the bulk atom in a fcc crystal structure can thus be written as $12f$. From literature it is known that the cohesion energy for Cu in the bulk (E_{coh}^B) is -3.48 eV [27, 48].

If the (111) surface of a fcc crystal consists of an adatom, the adatom have a maximum of three neighbouring atoms, and thus it can form a maximum of 3 bonds. Therefore E_{coh}^{adatom} is equal to $3f$ for an adatom of the (111) surface. With **equation 3.3** the vacancy formation energy in the bulk of a (111) single crystal, can be calculated as $9f$, which is equal to 2.61 eV. In a similar manner, the vacancy formation energy for a fcc crystal with a (110) surface can be calculated as 2.03 eV.

Surface orientation	Bonds in the bulk	Bonds with adatom	E_v (eV/vacancy)
(111)	12	3	2.61
(110)	12	5	2.03

Table 1: This table shows the difference in the vacancy formation energies of the (111)- and the (110) surfaces in Cu.

According to the calculated values in **table 1**, the vacancy formation energy (E_v) of the (111) surface is approximately 29% higher than that of the (110) surface. That means that the concentration vacancies in the bulk of the (111) surface is lower than that in the bulk of the (110) surface. According to a calculation done by Terblans [27, 50], the difference in the activation energy (Q) under the (110) surface and the (111) surface is approximately 17%.

In the next paragraph the influence that vacancies have on the diffusion coefficient is discussed.

3.4   The Influence of Vacancies on the Diffusion Coefficient

According to the vacancy diffusion mechanism, the diffusing atoms are in lattice positions and can only jump to another lattice position given it has enough energy and the lattice position is vacant.

The energy that an atom needs to deform the crystal and therefore jump to the neighbouring vacancy is called the migration energy (E_m).

An atom in a solid, vibrates at its lattice position with frequency v_0. At relatively low temperatures (< 300 K) the energy (vibration amplitude) of an atom is very small and therefore it can't jump to a vacant lattice position. For a fraction of the time, that is given by the Boltzmann distribution, the energy of the atom is equal to the migration energy (E_m) and the atom can jump. Therefore, for an atom that collides v_0 times per second against the energy barrier wall (E_m), the atom can thus jump over the energy barrier wall $v_0 e^{-E_m/RT}$ times per second. Terblans [27] showed that the Arrhenius equation can be written in a form where the migration energy and the vacancy formation energy are included:

$$D = \left(\frac{zv_0 d^2}{6}\right) e^{-(E_m + E_v)/kT} \tag{3.4}$$

where z is the number of neighbouring atoms and d the distance between two neighbouring atoms.

From the derived Arrhenius equation above it follows that:

$$D_0 = \frac{zv_0 d^2}{6} \qquad \text{and} \qquad Q = E_m + E_v \tag{3.5}$$

According to the derivation in **paragraph 3.3** the vacancy formation energy E_v is dependent on the surface orientation and thus the activation energy Q must also be surface orientation dependant.

From **equation 3.4** the diffusion coefficient can be written as:

$$D = D_0 e^{-(E_m + E_v)/kT}$$

$$= D_0 e^{-E_m/kT} e^{-E_v/kT}$$

$$= D_0 e^{-E_m/kT} X_v \tag{3.6}$$

where X_v is the vacancy concentration in the bulk of the crystal.

This means that the bulk diffusion coefficient, among others, is determined by the vacancy concentration in the bulk of a crystal. It has been shown above that the vacancy concentration in the bulk is influenced by the surface orientation. Therefore it is evident that the bulk diffusion coefficient is influenced by the surface orientation of the crystal.

The following two chapters describe the newly built annealing system and experimental setup and procedures, used to obtain experimental results supporting the theory that the surface orientation of a crystal influences segregation.

Chapter 4

A Pressurized Ar filled Annealing System

4.1.   Introduction

The annealing stage of segregation research is an important part of the preparation process of samples, thus this annealing system was designed and built. In segregation studies, researchers [27, 28, 51, 52, 53] often make use of diffusional doping in single crystals. Annealing the crystal is a critical step in the preparation of the specimen, as it may oxidize (even at low O_2 partial pressures) and destroy the near surface crystalline structure [54 – 56]. Liu et al. [57] also showed that crystals annealed in different gas atmospheres have different corrosion resistance. When doping crystals with elements of a low diffusion coefficient (D) (i.e. Sb and Sn in a Cu matrix), it is necessary to anneal the crystal for long periods of time at high temperatures to get a homogeneous distribution [58] (see **equation 5.1** in **chapter 5**).

After Sb has been evaporated onto the back face of the bi-crystal, it needs to be annealed, for a long period of time (~20 days) at high temperatures (1173 K), to enable the Sb on the surface to diffuse homogeneously through the Cu bi-crystal.

The previous method of annealing, in the Department of Physics at the University of the Free State, was done by placing the crystals with the adhered evaporant inside a quartz tube that had two protruding openings as is shown in **figure 4.1**. A steady but a slow flowing Ar gas source was connected to opening A. When the entire tube was filled with Ar after 2 minutes, opening B was heated till it became soft and was clamped and sealed. With the Ar gas still flowing but at a reduced rate, tube A was also quickly sealed [27, 33]. This method of annealing did not always leave the crystals unoxidized, as the possibility that there was a leak

was relatively high. The quartz tube described above is not commercially available and thus a glass blower that can work with quartz (which is very scarce) is needed to make and seal such an apparatus. A new custom built annealing system, which enables one to anneal samples at pressures above atmosphere, is described here.
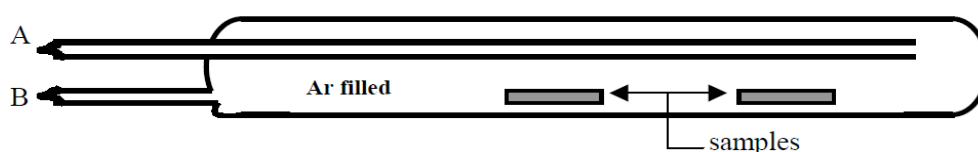

Figure 4.1: Quarts tube used for sealing crystals in an Ar atmosphere.

4.2.   The Mechanical Setup

The main component of this apparatus (see **figure 4.2**) is the quartz glass tube. This tube has a 36 mm outside diameter, 2 mm wall thickness and 900 mm length. The tube is mounted inside a furnace with resistive heating elements, which has a temperature controller capable of regulating temperatures to 1473 K. The ends of the tube protrude 20 cm on each side of the furnace, which is long enough to prevent the ends of the tube to reach temperatures above 373 K. This allows for standard conflat (CF) 40 metal flanges to be connected in a novel way to the ends of the tube using double viton o-rings at the metal tube end (see **figure 4.2**). This protrusion thus protects the viton o-rings from thermal excursions, as this will occur at approximately 473 K [59], and keeps the temperature of the stainless steel flanges relatively low ($<$ 323 K) to inhibit out gassing since stainless steel has the disadvantage of H_2 out gassing (but not exclusively) at an approximate rate of 1.5×10^{-16} Torr.ℓ.s^{-1}.cm^{-2} at 373 K [60]. The gas responsible for oxidizing the crystal inside the quartz tube is O_2 and since H_2 has the highest out gassing rate, from stainless steel, the out gassing of O_2 would be much lower at that temperature.

On the one end of the quartz tube a high purity, high pressure Ar gas cylinder is connected via a flow control valve, an inlet valve, a thermocouple pressure gauge and a CF 40 T-piece. On the opposite end, a rotary vane pump and a turbo molecular pump are connected via a manually controlled valve and a CF 40 cross. Also connected to the cross are a RS pressure transducer and a blank flange for sample introduction.
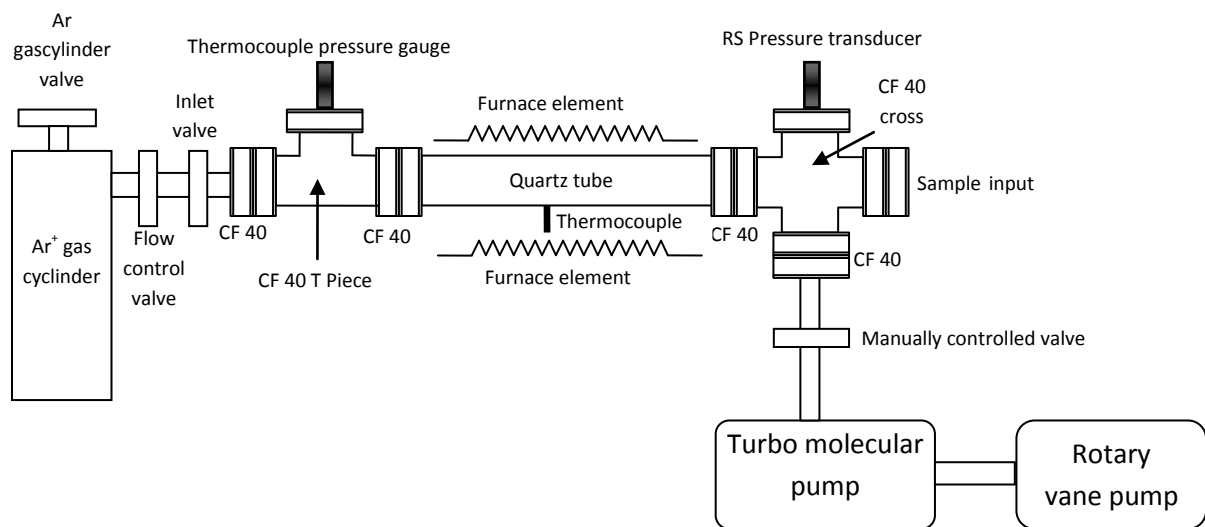

Figure 4.2: The mechanical setup of the annealing system.

The glass to metal connection makes use of a custom made stainless steel flange consisting of a groove to hold one viton o-ring in place over the quartz tube and a sloped end for the other viton o-ring to be screwed tighter against the tube as seen in **figure 4.3**.
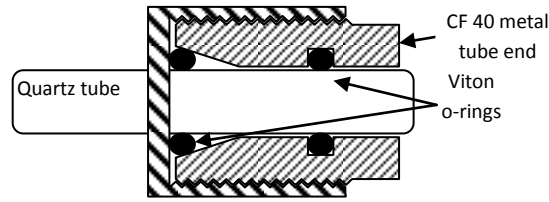
Figure 4.3: The glass to metal connection, indicating the positions of the viton o-rings.

4.3.   The Electronic Control Unit

An electronic control unit was designed and programmed, using a PIC 16F877 programmable EEPROM, to allow for input of a user defined pressure, to measure the pressure inside the tube, and switches the power to the furnace using a solid state relay (see **figure 4.4**). The unit also keeps record of the annealing time and presents a $0 - 10V$ output, proportional to the gauge pressure.
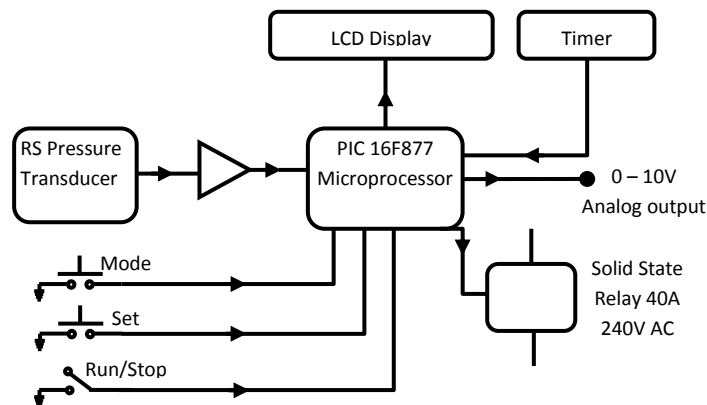

Figure 4.4: Schematic diagram of the electronic control unit.

Once the user defined pressure is set, the unit compares this pressure to the pressure inside the quartz tube. When the pressure inside the tube is higher the unit switches the power to

the furnace and starts the timer. When the pressure drops below the set pressure, which is an indication of a leak, the control unit cuts the power to the furnace and stops the timer. In the event of a power failure the unit switches to a 9V battery backup, to preserve the annealing time recorded.

4.4. Experimental Results and Discussion

After the apparatus was assembled the first step was to check the tightness of the system at room temperature. The tube was backfilled to a gauge pressure of 530 Torr and all valves closed. The pressure inside the tube was monitored as a function of time (see **figure 4.5**). The pressure difference in the time intervals II, III, V and VI was due to day / night room temperature changes (this was done in winter and thus the temperature gradient was high). The results show an average decrease in the gauge pressure of 84 Torr over a period of 6000 minutes, which is a flow rate of 1×10^{-13} Torr.ℓ.s^{-1}. The small change in the pressure over that period of time (comparable to typical annealing times) confirms the tightness of the vacuum components and connections.
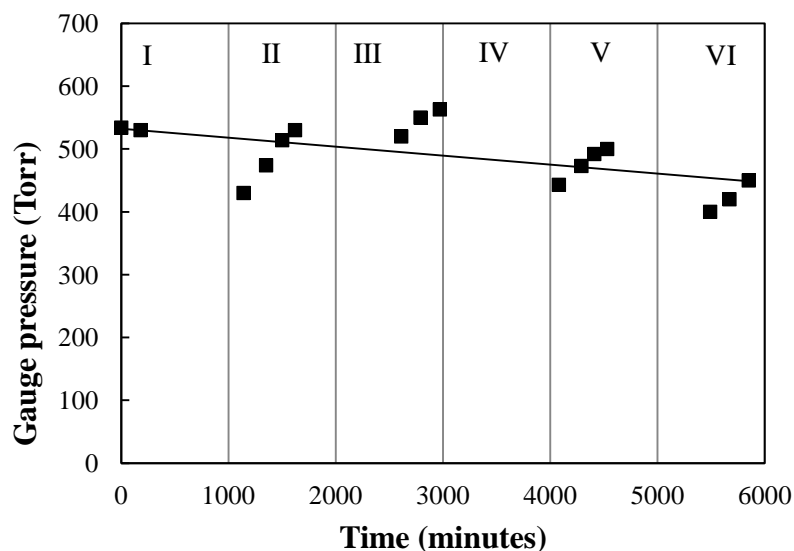
Figure 4.5: The integrity of the vacuum in the system shows that it can keep high pressures for long periods of time.

The next step was to determine, during pump down while the tube is under vacuum, what contaminants are present by determining the partial pressures of the gasses present in the tube. A gas analyzer was attached to the CF 40 cross (at the sample input), the system was pumped down and a spectrum of the partial pressures present in the tube (**Figure 4.6**) was obtained at 3.32×10^{-7} Torr.
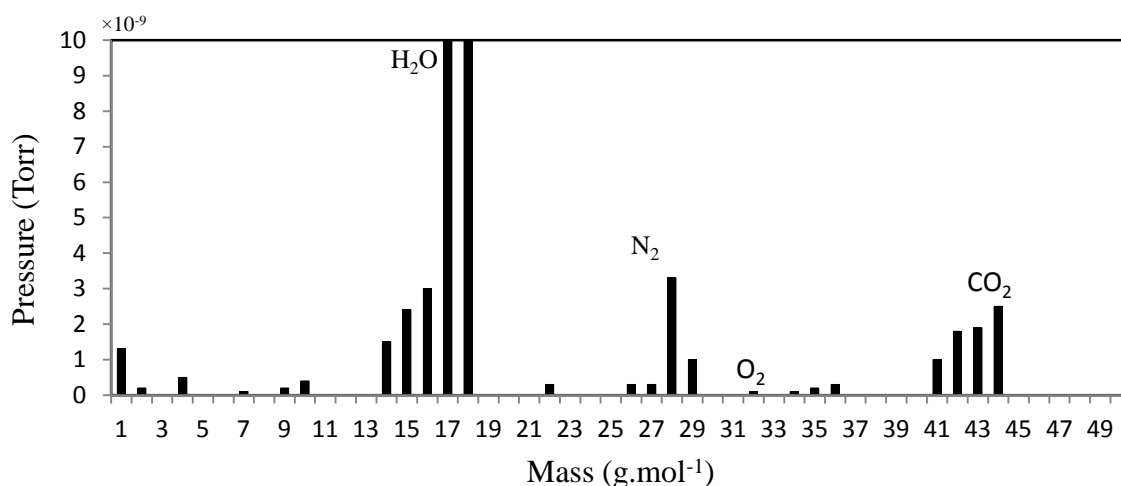
Figure 4.6: Partial pressures inside the tube at a total pressure of 3.32×10^{-7} Torr.

Figure 4.6 shows O_2, which has an atomic mass of 32 g.moll^{-1}, having a partial pressure of less than 1×10^{-9} Torr inside the tube while the tube was under vacuum. When single crystals are annealed, the main concern is that the crystal will oxidize and therefore it is ideal if the partial pressure of O_2, inside the tube, is very low as it is shown in **figure 4.6**.

According to **table 1** the maximum gauge pressure the tube can withstand is 2280 Torr. Using Gay - Lussac's law, the tube can be backfilled to a gauge pressure of 760 Torr Ar at a minimum temperature of half the annealing temperature, which will allow for the increase in pressure at higher temperatures as well as accommodate higher out gassing rates.

Breaking stress, tensile	**5 kg.mm^{-2}**
Breaking stress, compression	**200 kg.mm^{-2}**
Young's modulus	**E = 7200 kg.mm^{-2}**
Poisson coefficient	**V = 0.16**
Maximum gauge pressure (P_{max})	**15200 Torr**
P_{max} for this system	**2280 Torr**

Table 4.1: Technical data for the quartz tube [61].

A dummy annealing run was followed, without samples in the annealing system. The temperature was increased to 1223 K and the pressure increased to a maximum of 1380 Torr.

The gauge pressure was recorded as a function of the tube temperature and compared to the calculated pressure obtained from the Gay-Lussac law (see **figure 4.7**). This showed that the gauge pressure was approximately 200 Torr more than the calculated gauge pressure. This difference in the measured and calculated gauge pressure is due to out-gassing inside the tube.
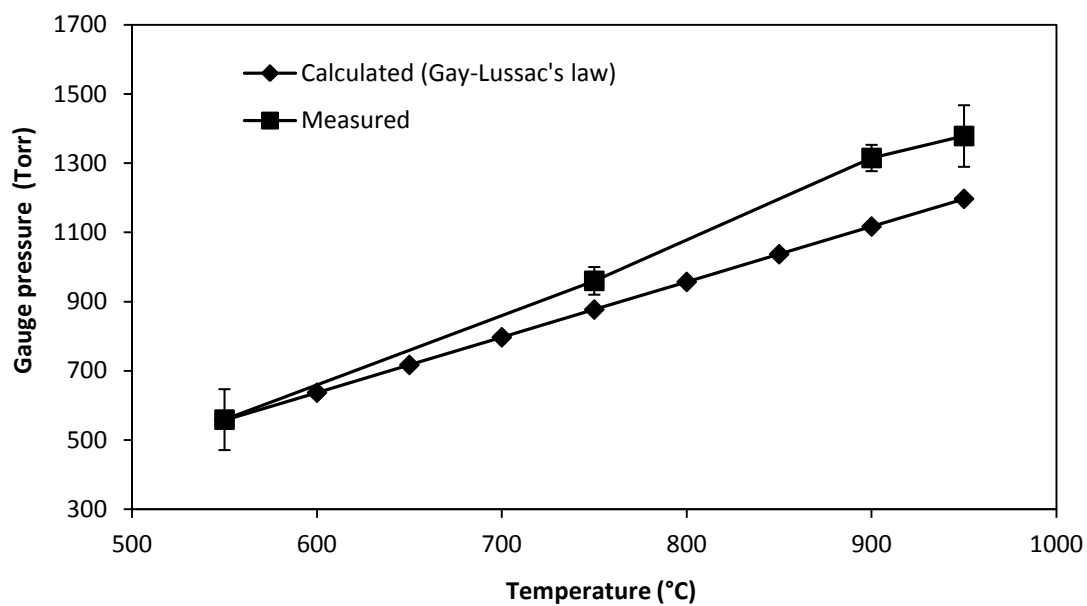
Figure 4.7: The gauge pressure as a function of temperature.

After the above procedure was completed, the tube was allowed to cool down to room temperature and the gauge pressure was again recorded as a function of temperature and Gay-Lusac's law was used to calculate the actual temperature inside the tube (see **Figure 4.8**).
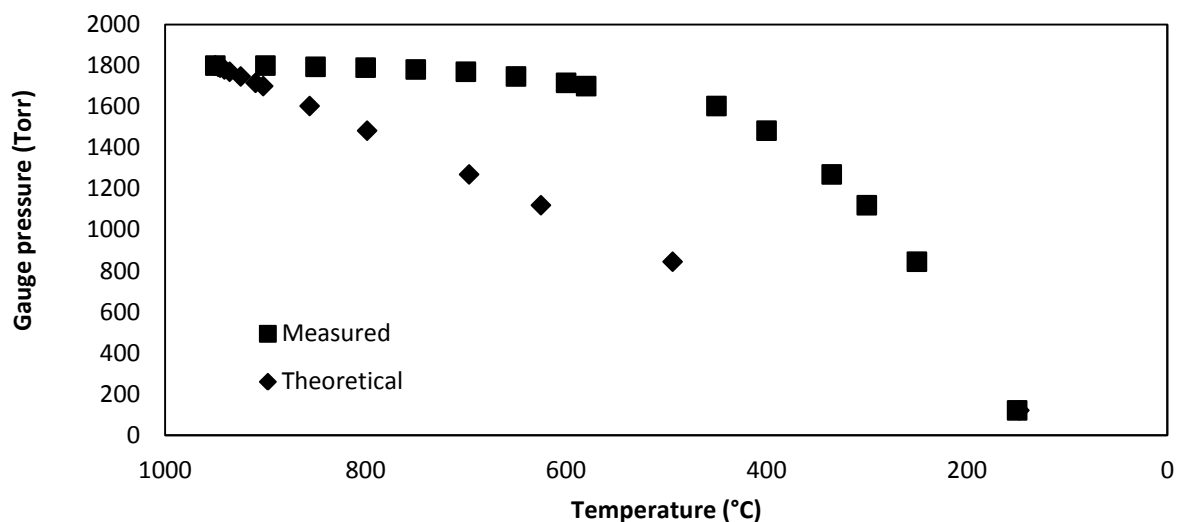
Figure 4.8: The gauge pressure as a function of temperature.

From **figure 4.8** it is seen that the temperature determined by the thermo couple of the furnace (TC1), outside the tube, does not represent the actual temperature inside the tube, but rather the surface temperature of the tube. The actual decreasing rate of the temperature inside the quartz tube is much slower than what is calculated. A thermocouple was attached to a polycrystalline Cu sample and placed inside the tube (TC2). Ar gas was allowed to flow through the tube at a flow rate of 5 l.min^{-1} and the temperature (TC1) was increased to 873 K in different steps. While the temperature was increased the surface temperature of the Cu sample (TC2) and the tube was monitored (TC1). When the temperature is increased by 373 K (TC1) the temperature inside the tube (TC2) overshoots with 40 K $\pm$ 10 K, after which it will decrease. When the oven temperature (TC1) is kept constant at 873 K the actual temperature inside the tube (TC2) is 893 K $\pm$ 5 K.

To determine the effect of the Ar atmosphere on crystals inside the tube during annealing, the following standard procedures were used to flush (purge) the system and anneal

polycrystalline Cu samples (Cu) and Cu polycrystalline samples doped with Bi (CuBi). CuBi was used as this was readily available in the department.

The Cu samples were introduced via the CF 40 cross to the centre of the quartz tube where the furnace thermo couple is positioned. The Ar gas cylinder valve, the inlet valve and the manually controlled valve were opened. The flow rate valve was adjusted for a 3 ℓ.min^{-1} Ar gas flow rate and the system was allowed to purge for 10 minutes. The turbo molecular pump was started and the inlet valve closed. Pump down was allowed for 10 minutes after which the temperature was increased to 373 K to allow for higher rates of out gassing. The manually controlled valve to the turbo molecular pump was closed and the inlet valve to the Ar gas was opened simultaneously, backfilling the tube to a gauge pressure of 500 Torr. This cycle was repeated until a temperature of 773 K was achieved. After this cycle, the gauge pressure was at 500 Torr and the temperature at 773 K. The temperature was then increased to 1223 K and the Cu samples were annealed for 3850 minutes at this temperature. After annealing, the tube was allowed to cool down to room temperature before the samples were removed and transferred to the XPS surface analysis chamber.

The annealed Cu samples were mounted in a PHI 5400 ESCA vacuum chamber with base pressure $< 8 \times 10^{-9}$ Torr. X-ray Photoelectron Spectroscopy (XPS) was performed *in situ* using a non monochromatic magnesium (Mg) K$_\alpha$ source (1253.6 eV) and a concentric hemispherical sector analyser (CHA) with a pass energy of 17.9 eV and a scan rate of 0.1 eV per 650 milliseconds. The X-ray source was operated at a power of 300 W and the electron take off angle was fixed at 45° for all analysis. The binding energy scale was calibrated with Cu 2p$_{1/2}$ (953 eV), Cu 3p$_{3/2}$ (933 eV) and Au 4f$_{7/2}$ (84 eV) peaks [62]. Ion Ar$^+$ sputter cleaning were done for 5 minutes with a 2 keV beam energy and a 2 x 2 cm^2 raster.

The Cu polycrystalline samples

During the transfer of the samples to the XPS system, a thin layer of "normal" surface contaminants (O_2 and C) adhered to the surfaces of these samples. This thin contaminant layer could easily be removed by means of sputtering the surfaces with 2keV Ar ions for approximately 5 minutes. The binding energy peak positions of Cu $2p_{1/2}$ (953 eV) and Cu $3p_{3/2}$ (933 eV) for the test samples were compared with the binding energy peak positions of the clean Cu polycrystalline sample which was used to calibrate the XPS system (see **figure 4.9**). It is clear from the graph that no detectable changes in the chemical composition of the Cu were measured and that the system can be used with an acceptable small risk of oxidation during annealing.
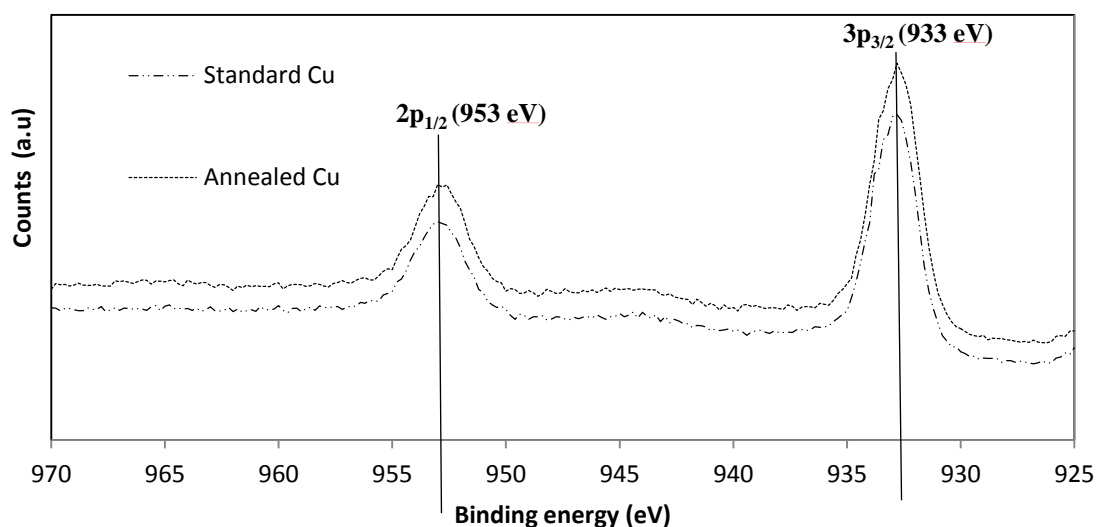

Figure 4.9: A comparison between the XPS spectra of a clean Cu and a Cu sample annealed for 3840 minutes at 1223 K. The spectra were subjected to x-ray line deconvolution and satellite subtraction.

The Cu polycrystalline samples with the Bi evaporant

After this annealing process was successful, a thin layer, 15 kÅ of Bi, was evaporated onto the Cu crystals by means of Electron Beam Physical Vapor Deposition and annealed (using the same procedure described above) at 538 K for 11 days with a final temperature of 1223 K for 3 days. The chosen temperatures were the result of the melting temperatures of Bi and Cu (544 K for Bi and 1356 K for Cu). The annealed CuBi samples were also mounted in the PHI 5400 ESCA vacuum chamber and the same experimental parameters as mentioned above was used to calibrate the XPS system.

A spectrum of the Cu(Bi) surface was obtained without sputtering (see **figure 4.10(a)**). The spectrum shows "normal" surface contaminants such as O_2 and C. Ar sputtering was done for 5 minutes with a 2 keV beam energy and a 3 x 3 cm^2 raster. This spectrum is shown in **figure 4.10(b)** showing no contaminants. After the sample was sputtered the temperature was raised to 873 K for 1 hour, allowing Bi to segregate (see **figure 4.10(c)**). Again no contaminants are present, indicating a successful annealing.

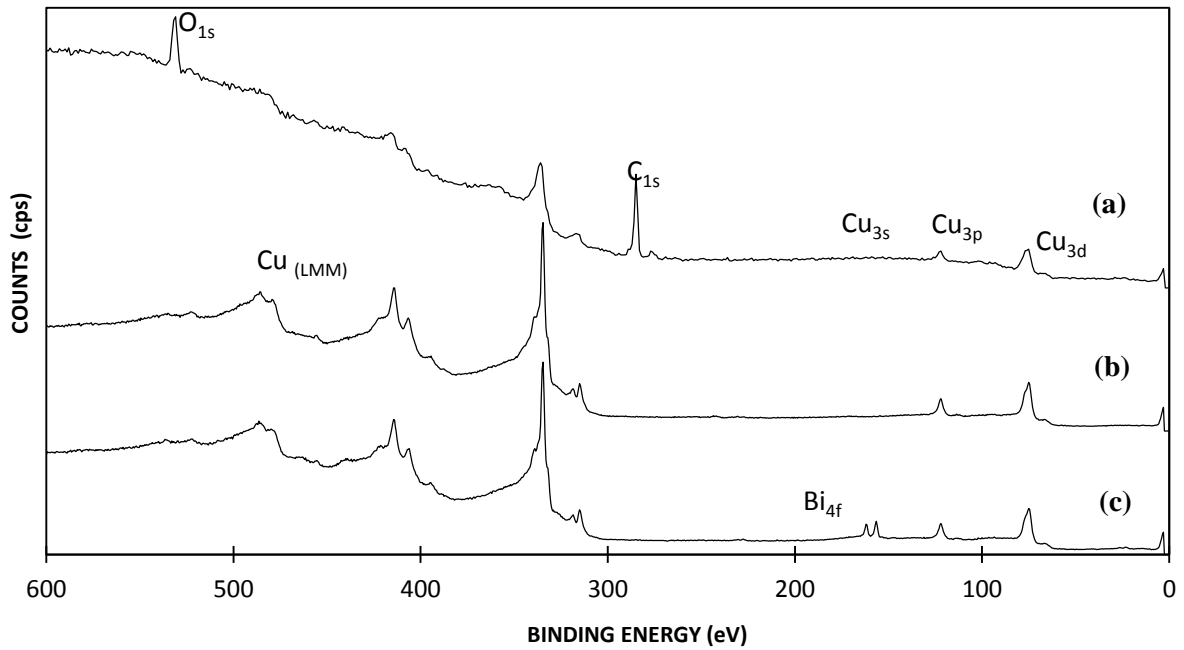**Figure 4.10:** XPS spectra (600 eV – 0 eV) of the Cu(Bi) as it came from the annealing system (a), after sputtering for 5 minutes (b) and after 1 hour at 600 °C (c).

It is clear from the spectra in **figure 4.10** that the Cu crystals were doped, with Bi, successfully and that no contaminants are present in the bulk and therefore the system can be used to dope crystals with an acceptable small risk of oxidation during annealing.

4.5.   The Proposed Annealing Procedure

A proposed general annealing procedure followed from these successful results:

1. Place the samples inside the quartz tube at the centre where the thermocouple of the furnace is positioned and fasten the blank flange.

2. With all valves open purge the system, with Ar flowing through the tube at a rate of 3 $\ell.min^{-1}$, for 10 minutes.

3. Close all valves and start the turbo molecular pump.

4. Open the manually controlled valve to the turbo molecular pump and allow pump down for 10 minutes.

5. Increase the furnace temperature with 100 °C.

6. Close the manually controlled valve to the turbo molecular pump and open the inlet valve to the Ar gas simultaneously, backfilling the tube to a pressure of approximately 500 Torr.

7. Repeat steps 4 to 5 until a temperature of half the annealing temperature is achieved.

8. After the annealing procedure is completed the temperature is allowed to decrease to room temperature after which the crystals are removed from the annealing system.

4.6.   Conclusion

An annealing system is designed and built that addresses various shortcomings in this laboratory's annealing procedures. The system uses standard CF connections and fittings, making it reusable in the long run with good pressure integrity and low out gassing rates. It is easy to assemble and disassemble, allowing the stand alone furnace to be used for other

purposes. The custom build electronic control unit is user friendly, measures the high pressure inside the quartz glass tube and allows for a 0 - 10V recorder output and records power failures and annealing time. The temperature measured inside the tube is 20 °C ± 5 °C higher than what is measured by the thermocouple of the oven, in the temperature range of 100 °C to 600 °C. XPS results confirmed that the high gauge pressure gas filled annealing system successfully protects the annealing samples (in a high Ar atmosphere) against possible corrosion because of atmospheric gasses. A general annealing procedure is deduced from the above experiments.

Chapter 5

Experimental Setup and Procedures

5.1   Introduction

The sample preparation and system setup plays an important role in experimental research (segregation studies). This includes how the data are accumulated, cleaning of the samples, determining the mass before and after doping the bi-crystal and the annealing process.

The first attempt to obtain segregation parameters from two different surfaces was done by Terblans [27]. This means measuring the segregation data from two different single crystals (two different surface orientations) at the same conditions i.e. the temperature of the crystals is recorded with the same thermo couple and the enrichment on the surfaces are measured at the same vacuum conditions with an e$^-$ beam with the same parameters, in other words the experimental conditions were the same. Unfortunately there are parameters that are difficult to control i.e. the room temperature (which can influence the performance of the spectrometer electronics), the thermal contact of the thermo couple on the crystal, the vacuum conditions, etc.

The experimental setup discussed in this chapter is a unique setup. The two single crystals are replaced by a bi crystal. The bi-crystal is mounted in front of the analyzer in such a way that the primary e$^-$ beam can be deflected from one surface orientation to the other. This allows segregation data to be accumulated from two surface orientations during one linear temperature run. The linear temperature run method is used as reported in reference [30, 63] and the temperature of the crystal was measured with a thermo couple as described by Terblans [27]. The segregation from the two surfaces are measured at exactly the same

experimental conditions, meaning that the segregation parameters from the two surfaces are directly comparable.

Another method of measuring on two different surfaces on one crystal was also explored. The idea was to use a stepper motor, controlled via a computer program, to physically move the crystal, while keeping the e$^-$ beam's position stationary.

The method described in this chapter proved to be the better method as it involved no development of external hardware and allows a much more accurate and repeatable measuring position.

The surface sensitive technique used to study the surface concentration, Auger Electron Spectroscopy (AES), and the newly developed program is also described.

5.2 The bi-crystal

The Cu bi-crystal bought from Mateck, in Germany [64], has the following specifications:

- a purity of 99.999 at. % Cu (5N)

- surface orientations (111) and (110) cut with an accuracy of 0.1°

- polished on one side to a roughness of 0.03 μm

- dimensions of, 1.15 mm thickness and a diameter of 8 mm

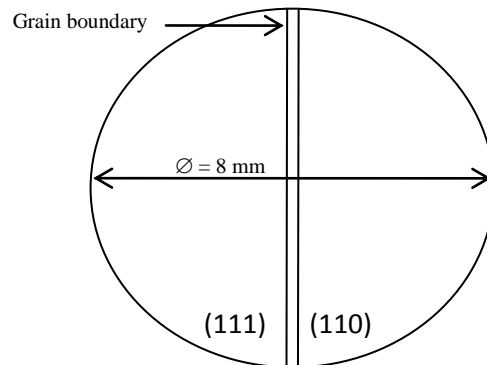- a grain boundary with a width of approximately 3 μm (see **Figure 5.2**).

Figure 5.1: A schematic diagram of the bi-crystal.

All measurements on the bi-crystal were done with the position of the specimen at the 2 keV primary electron beam elastic peak. This immediately makes the distance from the bi-crystal to the analyzer, along the analyzer axis, constant. It also ensures that the distance the electron beam is deflected on the bi-crystal is the same for the same potential difference on the deflection plates (see **paragraph 5.5** for deflection of e⁻ beam).

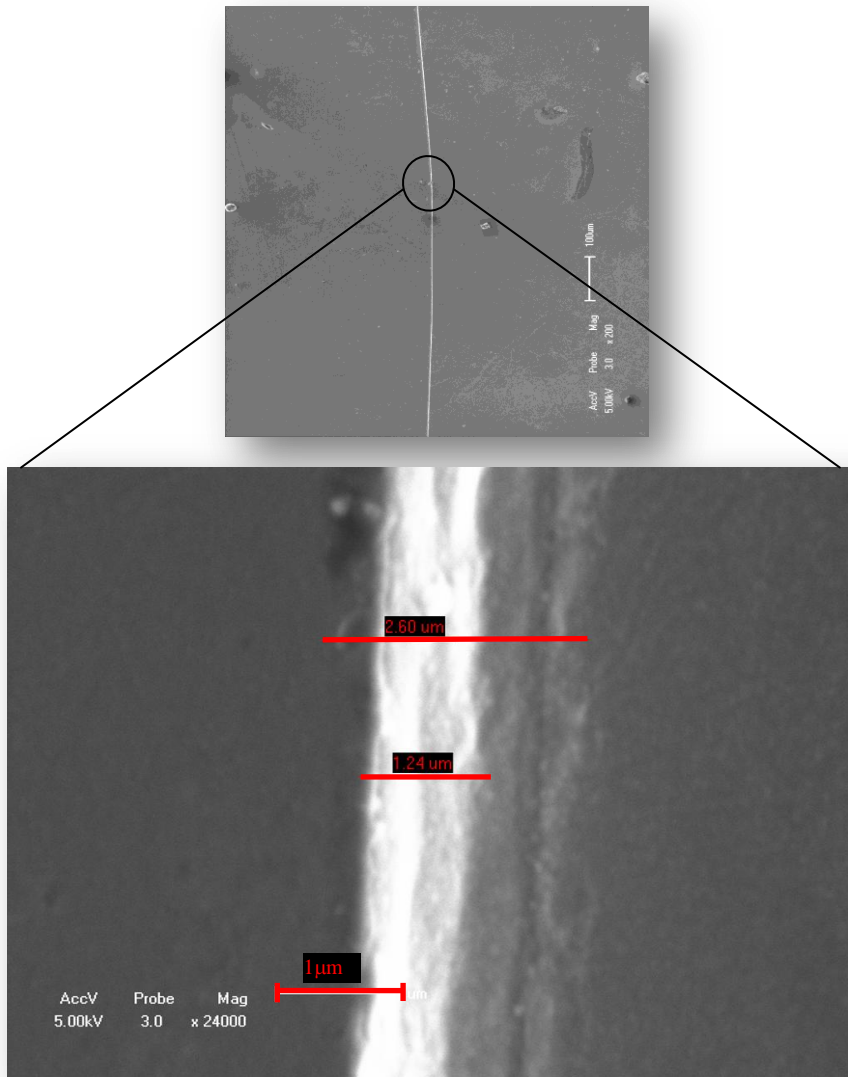Using the SEM images, the grain boundary of the bi-crystal was measured to be approximately 2.6 μm.

Figure 5.2: SEM images, using secondary electrons, of the grain boundary on the Cu bi-crystal with a maximum magnification of 2400×.

In order to determine the minimum distance the e⁻ beam must be deflected away from the grain boundary, segregation simulations were used. A rough estimate of the number of atomic layers, from the grain boundary, contributing to the flux of atoms to the surface from the bulk is equal to the ratio of the maximum solute coverage to the bulk concentration times 100 [28]. To safely assume that the impurity segregation flux is not influenced by the grain boundary segregation flux and a flux due to lateral surface diffusion, it is necessary to measure at a minimum distance of approximately 10.4 μm (5×10^4 atomic layers) away from the grain boundary. In order to minimize boundary effects during segregation

simulation the number of differential equations (N) must be chosen as large as possible (for a first order approximation this number of equations can be seen as the number of atomic layers from the surface [23]). Differential equations are not easily solved; therefore a lot of computer power is needed to solve a number of them in a reasonable amount of time.

5.3   Preparation of the Cu bi-crystal

A Cu polycrystalline rod (4N) and Sb granules (5N) were ordered from Goodfellow Cambridge Limited [65] and Mateck in Germany [64], respectively. Six dummy Cu polycrystalline samples were cut to similar sizes as the Cu bi-crystal (see **paragraph 5.2**) and mechanically polished, on one side, to 0.3 µm using a diamond suspension solution.

The bi-crystal was ultrasonically cleaned in methanol for 10 minutes and blow dried with N_2 gas. It was polished, on the back face of the crystal, up to 1 µm on a diamond suspended solution, again ultrasonically cleaned in methanol for 5 min and blow dried with N_2 gas and then weighed. The balance used was a calibrated Mettler M3 balance (see **table 5.1** for the mass before and after evaporation).
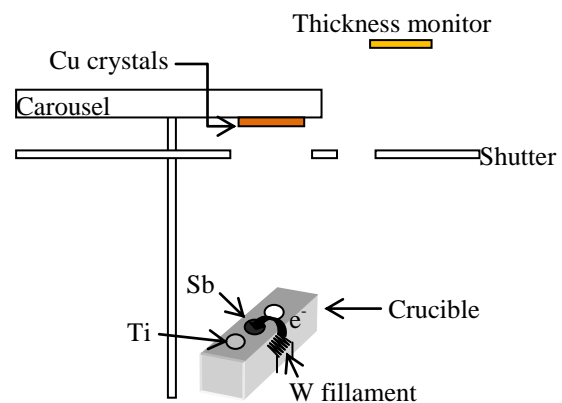
Figure 5.3: A photo and a schematic diagram of the evaporation system that was used to

evaporate approximately 20 kÅ thick layer of Sb on the back face of the Cu

crystals.

All crystals were mounted on a carousel and introduced into an evaporation chamber (see **figure 5.3**).

The evaporation chamber was pumped down (using a turbo pump), to a pressure of 2.6×10^{-5} Torr. A Ti sublimation pump was used additionally to obtain a pressure of 1×10^{-6} Torr. A thick Sb layer of approximately 20 kÅ was evaporated, simultaneously, onto the back faces of the crystals at an evaporation rate of approximately 5 Å.s^{-1}.

Shortly after the crystals were removed from the evaporation chamber they were weighed again to determine the mass of the evaporated Sb.

The Cu bi-crystal had a mass of 516.337 mg before evaporation. After evaporation the specimen with the adhered Sb layer, had a mass of 517.367 mg, giving an evaporated Sb mass of 1.030 mg.

Mass of Cu bi-crystal before evaporation (mg)	Mass of Cu bi-crystal after evaporation (mg)	Mass of Sb evaporated onto the Cu bi-crystal (mg)	Atomic Sb concentration in the Cu bi-crystal (at.%)
516.337 ($\pm$ 0.005)	**517.367** ($\pm$ 0.005)	**1.030** ($\pm$ 0.005)	**0.103** ($\pm$ 0.001)

Table 5.1: The mass of the Cu bi-crystal before evaporation, after evaporation and the mass

and calculated concentration Sb in the the bi-crystal.

The six Cu dummy polycrystalline samples went through the same procedures.

For the diffusional doping, a new annealing system was designed and built as part of this investigation (see **chapter 4**). This system allows the crystal to be annealed in an Ar atmosphere at relatively high temperatures for long periods of time.

The annealing procedure started by raising the temperature in steps of 10 K up to 863 K, after which the temperature was increased in steps of 1 K up to 873 K. The crystals were then annealed for three days at this temperature. This was done to ensure that the temperature in the tube stays below the melting point of Sb (903 K). The temperature was then increased to a final annealing temperature of 1173 K. The crystals were annealed at this temperature for 21 days to obtain a homogeneous distribution of at least 95 % (see **figures 5.4** and **5.5**). The homogeneous distribution was calculated with the equation in the book of Crank [40]:

$$C(x,t) = C_0 \sum_{n=-\infty}^{\infty} \left[\mathrm{erf}\left(\frac{h+2nL-x}{2\sqrt{Dt}}\right) + \mathrm{erf}\left(\frac{h-2nL+x}{2\sqrt{Dt}}\right) \right] \qquad (5.1)$$

where C_0 is the initial concentration on the surface, D the diffusion coefficient of Sb in Cu, t the annealing time, h the initial thickness of the evaporated layer on the surface and L the thickness of the crystal. The parameters used in the simulation were taken from [27].
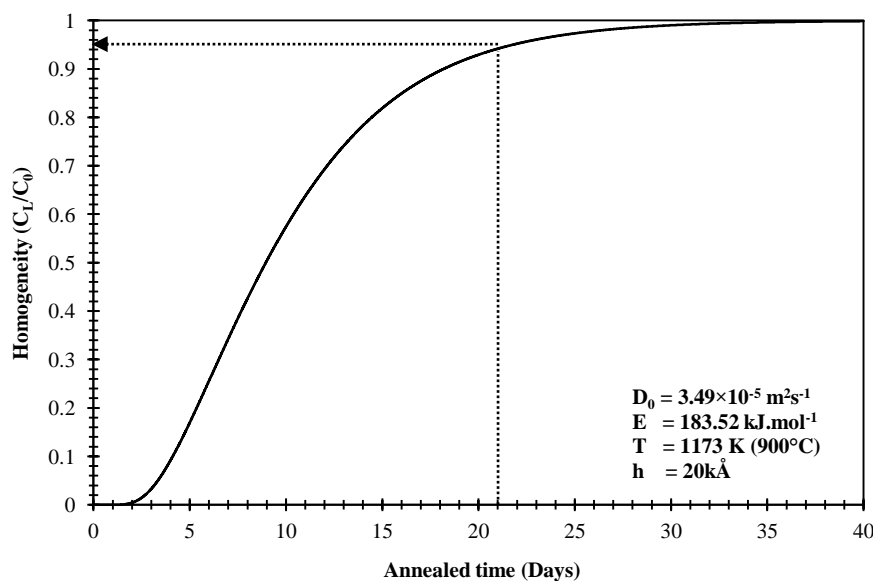
Figure 5.4: A graph of the Sb homogeneity in the Cu crystal as a function of annealing time at 1173 K.
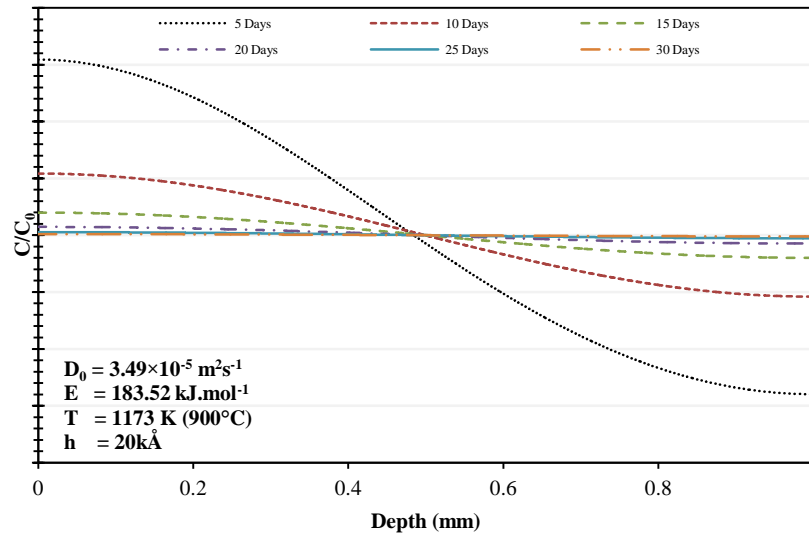

Figure 5.5: A graph of the Sb distribution in the Cu crystal annealed at 1173 K for different times.
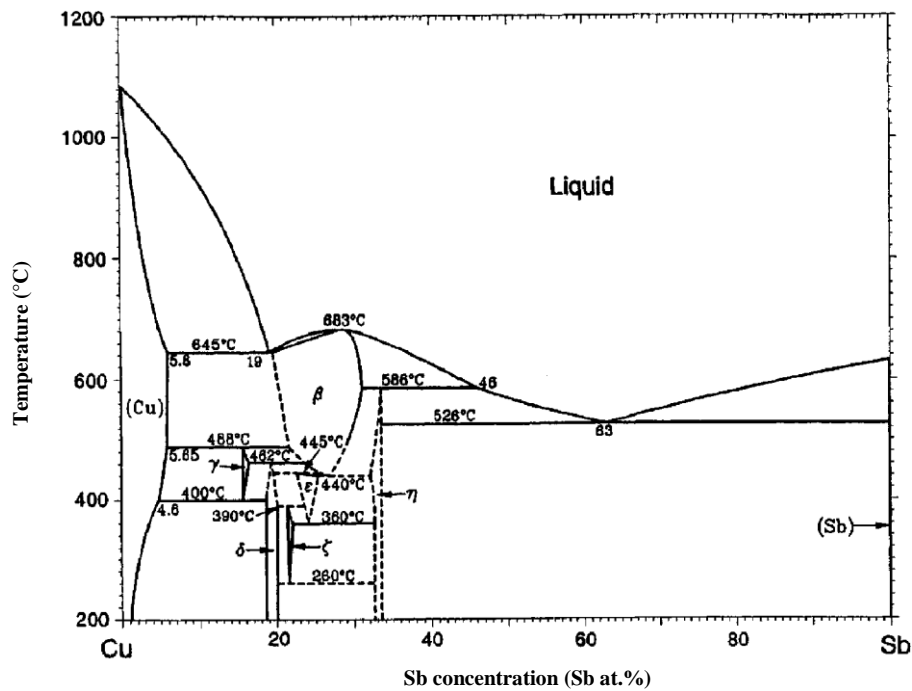
Figure 5.6: The phase diagram of CuSb, showing the solubility of Cu and Sb at the specified concentration.

The mobility of grain boundaries increases with increasing thermal energy, not only in polycrystalline materials, but in bi-crystals as well, as studied by Shvindlerman et.al. [15 – 17]. This may result in microstructure evolution and grain growth in polycrystalline samples and the possibility of migration of the grain boundary in a bi-crystal. No literature could be found on the effect of Sb impurity on grain migration in a Cu crystal. **Appendix A** is the result of a secondary study on the influence of Sb doping on the grain growth in a Cu crystal. The study indicated that by doping a Cu crystal with low concentrations Sb ($<$ 0.1 at. %) the crystal growth and thus the mobility of the grain boundaries are suppressed.

5.4   Auger Electron Spectroscopy (AES)

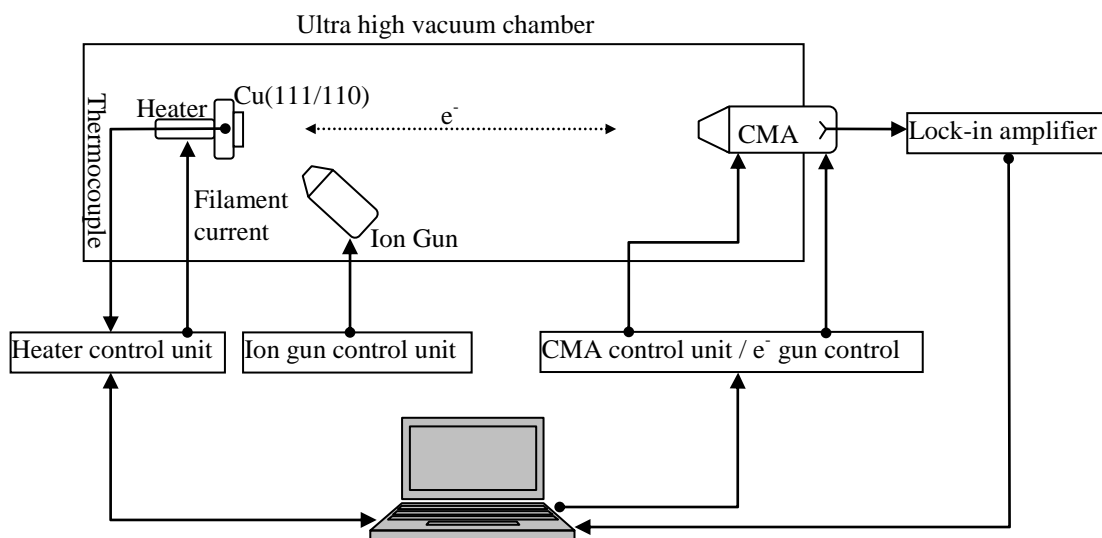The AES system consists of the following components (see **figure 5.7**):

Figure 5.7: A block diagram describing the computer controlled AES system that was used to accumulate segregation data.

1. An ultra high vacuum chamber connected to a turbo pump, which is used to obtain pre-vacuum conditions ($< 1 \times 10^{-6}$ Torr). The chamber also consists of an ion pump and Ti-sublimation pump used to obtain a pressure of $< 2 \times 10^{-8}$ Torr.

2. A Perkin Elmer 20-320A e⁻ gun and control unit providing the primary e⁻ beam in the AES. In this study, the primary e⁻ beam energy was set at 3 keV and the beam current at 4.5 µA. The filament current was set at 3.5 A and the emission current at 1.5 mA. The position of the sample was moved until it was on the focal point of the analyzer. The focal point is defined by elastically backscattered 2 keV electrons of the primary beam.

3. A Perkin Elmer 20-070 scanning unit. This unit is computer controlled so that the e⁻ beam can be scanned across the crystal, to obtain an absorbed current image.

4. A Perkin Elmer 15-110B single pass cylindrical mirror analyzer (CMA). The CMA aperture size was set to large (energy resolution 1.2%). This was done for a maximum e⁻ beam deflection and to still achieve relatively high yields.

5. A Stanford Research Systems, model PS325 / 2500 V – 25 W, high voltage power supply for providing the electron multiplier with 1200 V.

6. A Perkin Elmer 11-500A Auger System Control where the mode was set to external, in order for the unit to be controlled via a computer, and the modulation voltage was set to 2 eV, in order to improve the energy resolution due to the large aperture size. This modulation voltage is fed to the Lock-in-Amplifier.

7. A PHI 32-010 Lock-in-amplifier differentiating the Auger signal with a sensitivity of 10× and a time constant of 0.3 s. The time constant was set as specified, because the

scan rate was 2 eV.s^{-1} in order to increase the number of data points in the segregation profiles.

8. The PHI 20-115 Ion gun control unit and the PHI 04-177 Ion gun for cleaning the specimen surface. The vacuum chamber was backfilled to 5×10^{-5} Torr with high purity Ar-gas to obtain an ion beam current of approximately 100 nA with a 2 keV accelerating voltage and a raster of 3×3 mm^2, as measured with a Faraday cup.

9. The crystal was heated linearly with time, t, at a constant heating rate, α (see **equation 5.1**).

$$T = T_0 + \alpha t \tag{5.1}$$

The surface concentration was recorded as a function of time, t (or temperature T). T_0 is the starting temperature of the ramp [30, 63].

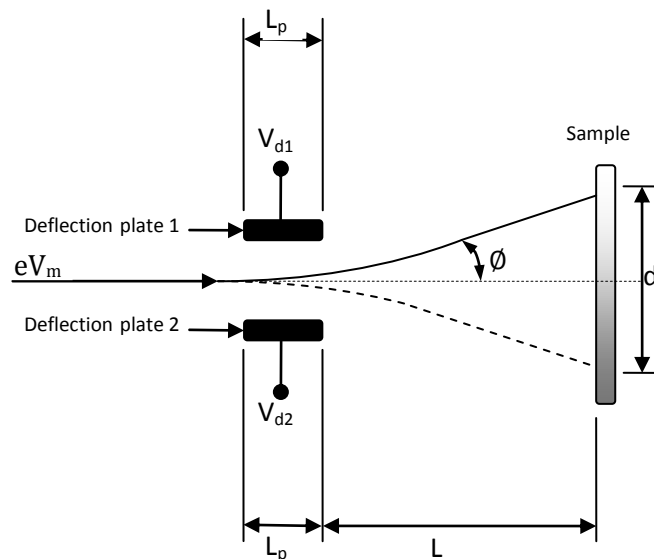## 5.5   Modification of the AES e$^-$ beam and Program Development

Figure 5.8: The deflection of an e$^-$ beam by means of deflection plates.

In the AES instrument the e⁻ gun is positioned coaxial in the analyzer. Apart from a condenser lens and objective lens, the gun is also fitted with two sets of deflection plates, perpendicular to each other and positioned at the exit of the gun. A first step in the modification of the e⁻ gun was to physically orientate the gun inside the analyzer, in such a position that the plates act in a vertical and horizontal direction, relative to the laboratory frame of reference. The factory electronics of the e⁻ beam was also modified to allow the horizontal and vertical deflections to be controlled independently by an external source. The amplification of this external voltage is such that a ± 10 V input results in a maximum deflection of the beam.

A voltage applied to the deflection plates will deflect the beam (see **figure 5.8**). The degree of the deflection is determined by the voltage on the plates and the energy of the electrons.

5.5.1 Program Development

The older version of the program, written on a Visual Basic 3.0 platform, used to control the AES system was not programmed to deflect the e⁻ beam during AES measurements. All AES measurements were taken with the beam in the central position. The software had to be modified to be able to take measurements on both orientations of the bi-crystal in a reasonable amount of time while the temperature of the crystal is ramped linearly.

A first step, in the program development, was to modify the program to be able to deflect the e⁻ beam say to orientation one, take an AES spectrum then deflect it to orientation two and take another AES spectrum. This deflection of the beam and the AES measurements are then repeated while the temperature of the crystal is ramped linearly. This ensures that the surface compositions of both orientations are measured by the same thermocouple and heated by the

same resistive source with the same electrical contacts throughout the measuring circuit and the same conditions for the spectrometer. A DAC (USB MicroDAQ, USB-30B-73R), from Eagle Electronics was used to control the AES system via a USB port. The program was developed on a Visual Basic 6.0 platform (see **figure 5.9**).

Figure 5.9: A screen image of the main window in the program.
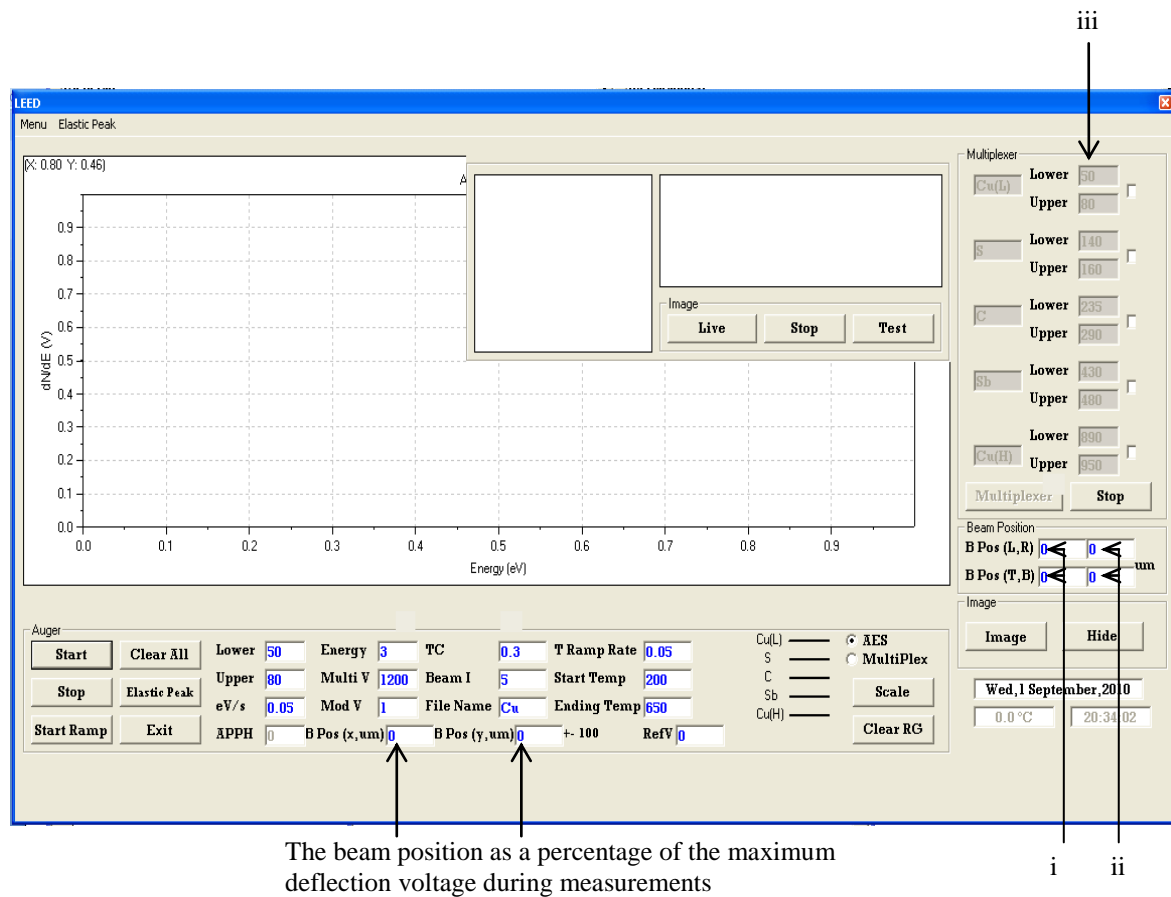
Because the deflection distance of the e⁻ beam is not the same at all beam voltages, the deflection is specified as a percentage, where -100 is the maximum position to the left and +100 the maximum position to the right (the same applies for the deflections in a vertical position). A Faraday cup was used to insure that the deflection of the e⁻ beam is horizontal.

By entering a +100 or -100 in the input boxes at (i) and (ii) (see **figure 5.9**) a signal is sent to the DAC which will in turn provide a voltage of either +10 V or -10 V, respectively. The outputs of the DAC are connected to the modified custom inputs at the back of the scanning unit which controls the potential differences on the deflection plates.

The position of the beam is expressed in the main window, (left or right (x), top or bottom (y)) i.e. (-100, 50) which means the beam position would be entirely left and a quarter from the top most position (see **figure 5.10**).
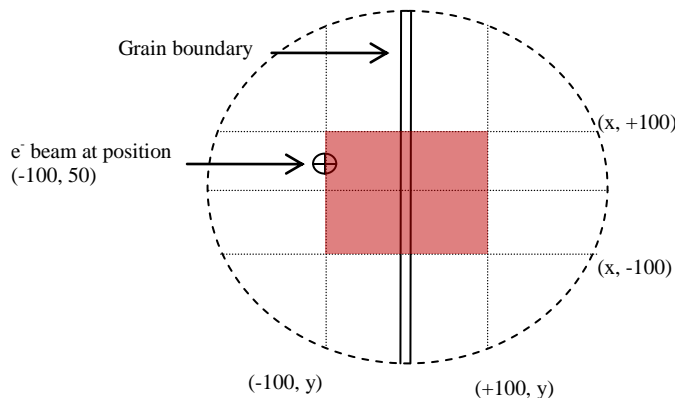
Figure 5.10: A schematic diagram showing the e⁻ beam on the bi crystal at position (-100, 50). The shaded area is where the e⁻ beam can be scanned across to obtain an absorbed current image. (not drawn to scale)

The temperature is controlled via a program written on the Visual Basic 3.0 platform on another independent computer. The AES computer that makes use of the new program developed for this study is synchronized (time) with the temperature computer. When the heating ramp is started the temperature computer signals the AES computer and the measuring process is started.

The program starts by using the values specified in the input boxes at (i) (see **figure 5.9**) to deflect the beam to the specified position, take the AES measurements in the energy ranges specified in the multiplex boxes at (iii). The program then uses the values specified in the input boxes at (ii), deflect the beam and take the AES measurements in the same specified energy ranges. After each deflection a settling time of 300 ms is allowed, before the Auger spectrum is recorded. This deflection procedure is repeated until the final ramping temperature is reached.

5.5.2   Determining the e⁻ beam Diameter and the Deflection Distance

Before the e⁻ beam diameter was determined it was focused by obtaining the best possible focused absorbed current image.

The e⁻ beam diameter was determined using a Faraday cup to measure the beam current and a micro-meter on the carousel to move the faraday cup perpendicular to the e⁻ beam. The e⁻ beam diameter and deflection distance were determined for the beam parameters specified in **paragraph 5.4**.
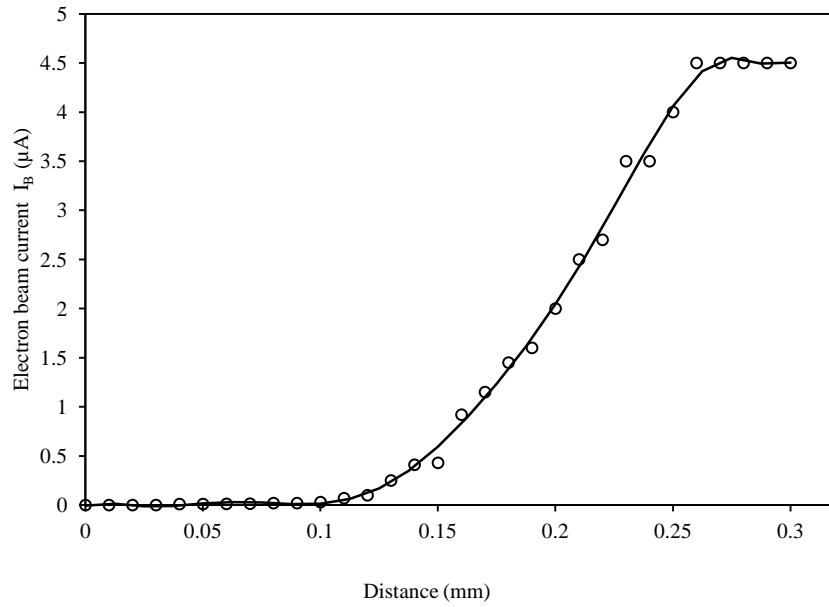
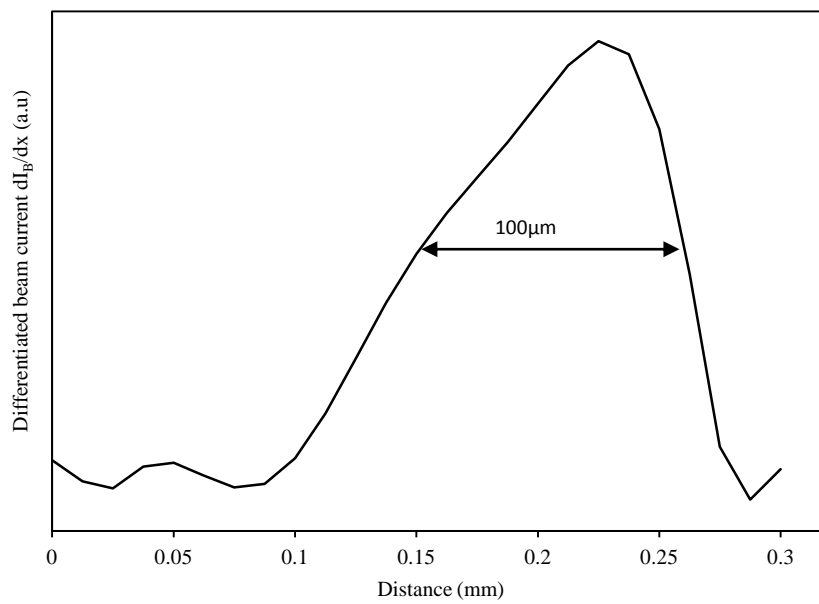**Figure 5.11:** Graph of the beam current versus the distance the faraday cup is moved.

Figure 5.12: Determining the e⁻ beam diameter.

A standard procedure [66] was used to determine the e⁻ beam diameter. A Faraday cup was moved horizontally and perpendicular to the e⁻ beam, and the e⁻ beam current was measured

as a function of distance (see **figure 5.11**). The diameter of the beam was determined by numerical differentiating the current from the Faraday cup with respect to position and taking the full width at half maximum (see **figure 5.12**). The focused beam diameter was determined as 100 μm.

It is important to know what the diameter of the focused e⁻ beam is, because it was necessary to calibrate the deflection distance scale, to ensure that when the electron beam is deflected away from the grain boundary, of the bi-crystal to either the (111) surface or the (110) surface, it is deflected far enough to ensure that grain boundary segregation does not influence the measurements. The procedure used to position the bi-crystal in front of the analyzer is discussed in **paragraphs 5.6** and **5.7**.

The Faraday cup was moved to the position where the middle of the e⁻ beam was on the edge of the Faraday cup (see **figure 5.13**).
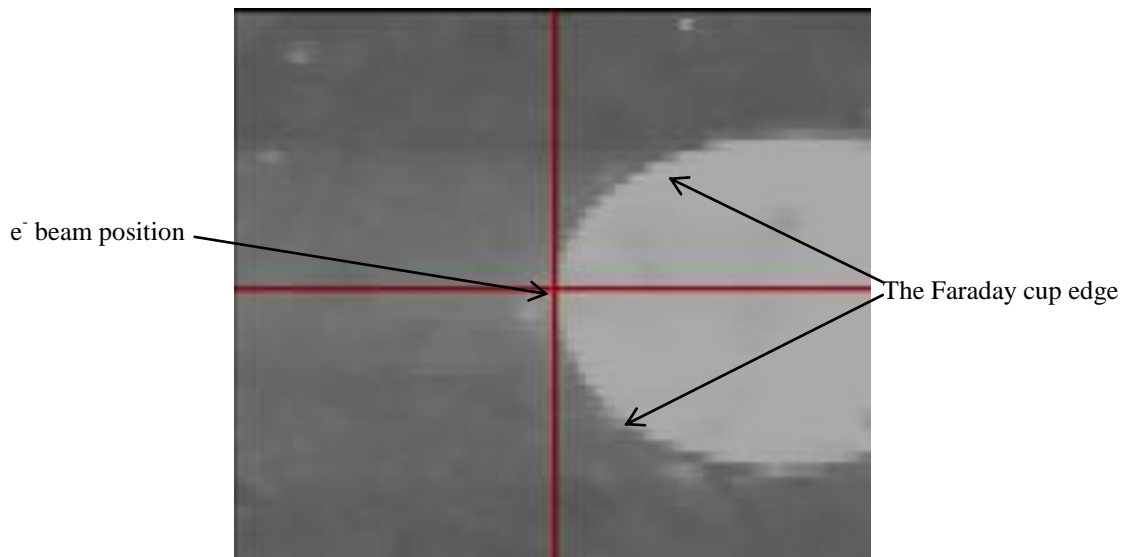
Figure 5.13: An absorbed current image showing the Faraday cup edge. The red cross indicates the position of the beam without deflection at (0, 0).

The beam was deflected to the maximum position left (-100, 0) and the Faraday cup was moved until the centre of the beam was on the edge of the Faraday cup. The same was done for the deflection of the beam to the right. The total deflection distance from (-100, 0) to (100, 0) is 1.7 mm with an average deflection distance of 0.4 mm for every (50, 0) step. The grain boundary width is thus relatively small compared to the deflection distance of the e⁻ beam, as discussed in **paragraph 5.2.**

The maximum width of the grain boundary of the Cu bi-crystal, as determined from SEM images (see **paragraph 5.2**), is 3 µm. If the crystal is moved in such a way that the grain boundary of the specimen is at the centre position of the e⁻ beam (0, 0), it is possible to deflect $\pm$ 0.85 mm, in a horizontal direction, away from the grain boundary. The effective distance away from the grain boundary is 0.8 mm (see **figure 5.14**). Thus, a deflection of 0.8 mm represents 4×10^6 atomic layers in the Cu bi-crystal, which are two orders of magnitude more than the 5×10^4 needed in the simulation (see **paragraph 5.2**).
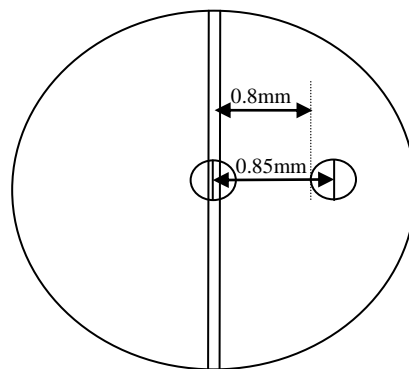
Figure 5.14: A schematic diagram to show the e⁻ beam deflection on the bi-crystal.

It is therefore concluded that the 1.7 mm that the e⁻ beam can be deflected is sufficient for the segregation measurements on the two different surface orientations without any interference from the grain boundary.

5.6   The Procedure for Positioning the Cu bi-crystal in Front of the Analyzer

To minimize the differences in the spectra of the two orientations due to the positional geometry of the Cu bi-crystal, the procedure below was followed:
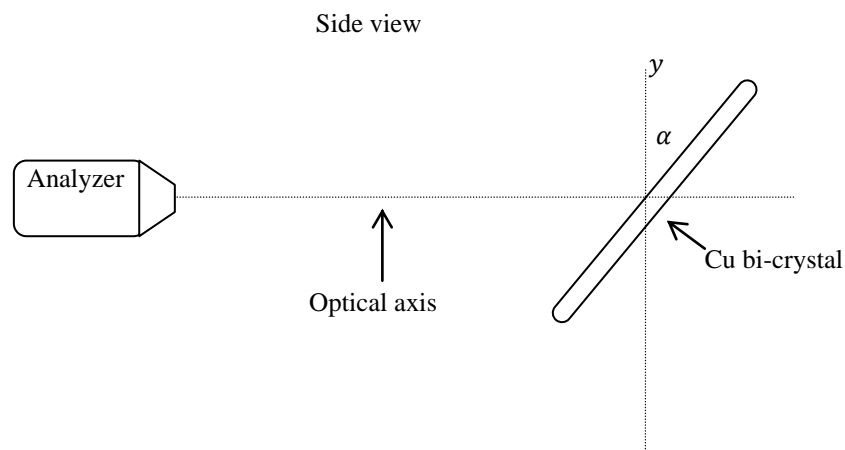
Figure 5.15: A schematic illustration of the bi-crystal in front of the analyzer as seen from the side.

1. The bi-crystal was mounted on the heater with the grain boundary in a vertical direction (y – direction) in front of the analyzer with an angle of $\alpha = 30°$ (see **figure 5.15**). This was necessary for sputtering purposes.

2. The crystal was moved to the elastic peak position, with the e⁻ beam undeflected in the (0, 0) position.
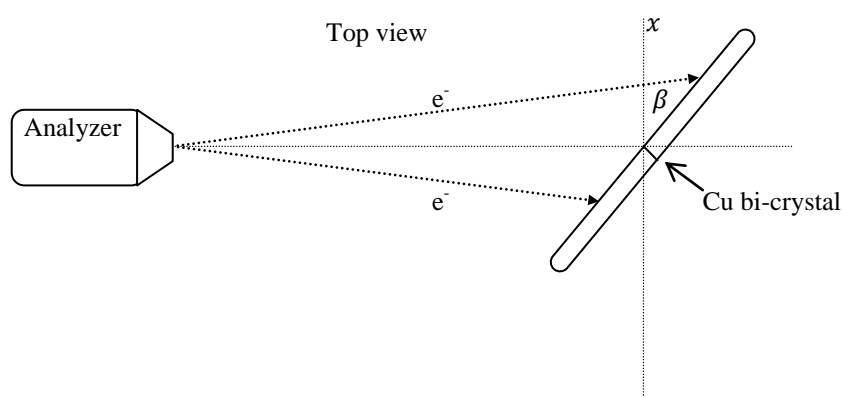
Figure 5.16: A schematic illustration of positioning the bi-crystal in front of the analyzer as seen from the top.

3. The crystal was positioned perpendicular in front of the optical axis of the analyzer. This was done by deflecting the beam from the middle position (0, 0) to either sides ((-100, 0) and (100, 0)) adjusting the crystal (β, see **figure 5.16**) about the vertical axis until the elastic energy positions were the same.

5.7 Identifying the Two Surface Orientations on the bi-crystal

The two surface orientations of the bi-crystal were identified using a method, where the equilibrium Sb coverage in the Cu surfaces is compared.

It has been shown previously that the maximum equilibrium Sb coverage in the Cu(111) and the Cu(110) surfaces are, respectively, 33 at. % and 50 at. % [51, 67 – 71]. The crystal was heated at 973 K for one day. This was done to ensure that the segregation in the Cu crystal was at equilibrium (maximum Sb coverage in the Cu surfaces). With the beam in the centre position (0, 0), the crystal was moved horizontally to either surface and an Auger spectrum was obtained (see **figure 5.17**). There was a 60 % difference in the Auger Peak to Peak Heights (APPH) of the spectra and therefore the Sb Auger spectrum from the surface with the smallest APPH was assumed the Cu(111) surface.
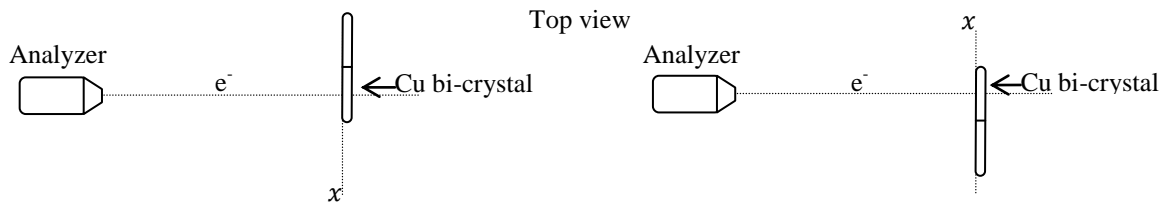
Figure 5.17: A schematic illustration of the method used to identify the two surfaces of the bi-crystal.

5.8   The Procedure for Recording the Segregation Data

More than one linear heating run [27, 63, 30], with different heating rates (0.05 $K.s^{-1}$, 0.75 $K.s^{-1}$ and 0.1 $K.s^{-1}$), was done on the bi-crystal and therefore the procedures, when determining the segregation data must be the same for every linear heating run to ensure that the parameters extracted are correct.

The e^- beam filament was switched on and adjusted to the specified beam parameters, at least 2 hours before any measurements, to allow the e^- filament to stabilize.
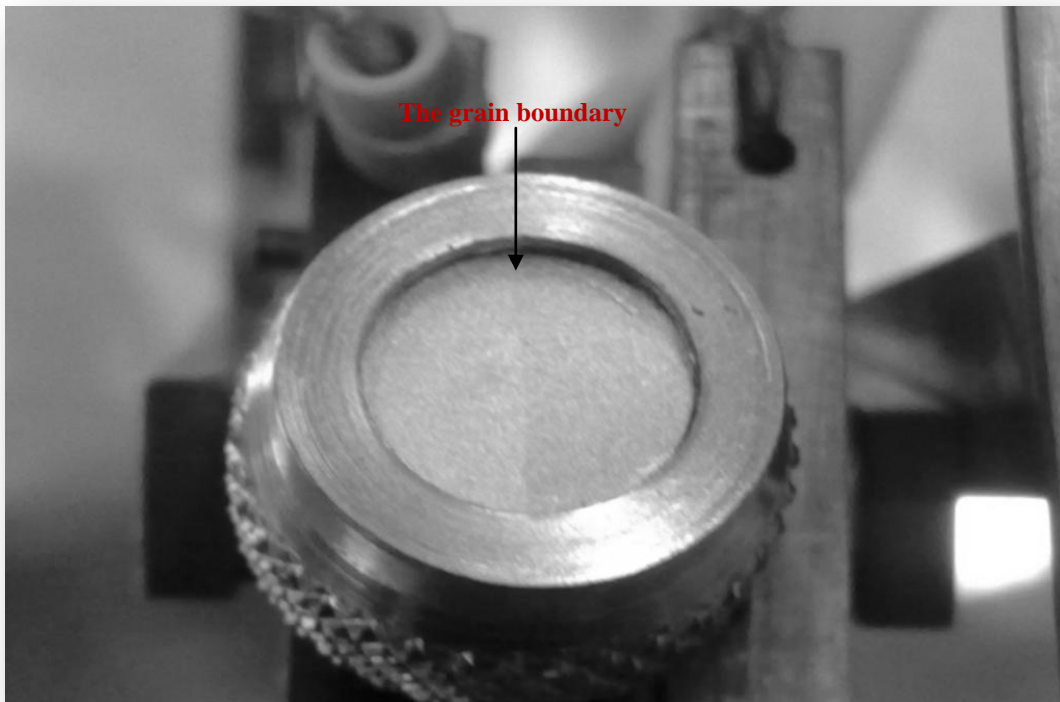
Figure 5.18: A picture of the mounted Cu bi-crystal.

Steps 1 to 9 were followed:

1. The Cu bi-crystal was mounted on the manipulator, on the heater with the grain boundary vertically in the middle (see **Figure 5.18**).

2. The vacuum chamber was pumped down to a base pressure of $< 2 \times 10^{-8}$ Torr.

3. The e⁻ beam current was set to 4.5 μA measuring the current in a Faraday cup.

4. The specimen was positioned in front of the analyzer (see **paragraphs 5.6** and **5.7**).

5. Before any measurements were done on the bi-crystal, it was cleaned, by Ar sputtering, of surface contaminants (C, S, O). The procedure described by Asante [28] was also used.

    i. The bi-crystal was sputtered at room temperature for 5 minutes using 2 keV Ar ions with an ion current of 100 nA rastered over an area of 3×3 mm^2.

    ii. It was then heated to a temperature of 823 K to desorb surface trapped O_2 and sputtered again for 5 minutes.

    iii. The temperature of the bi-crystal was increased to 923 K and annealed for 10 minutes without sputtering so as to level off any concentration gradient.

    iv. The crystal was then cooled down to 823 K and sputtered for 5 minutes at that temperature.

    v. The cycle (steps i and ii) was repeated six times before a clean surface was obtained.

6. The crystal was annealed at 973 K for 12 hours to allow for the vacancy concentration to reach equilibrium and for the vacancies to be distributed homogeneously in the crystal.

7. The crystal was allowed to cool down to a temperature of 473 K. Steps 6 and 7 were repeated to ensure that the vacancy concentrations in the crystal are the same at the start of each linear heating run.

8. The chamber was backfilled to an Ar pressure of 5×10^{-5} Torr and the surface of the bi-crystal sputter cleaned for 5 minutes (with 2 keV Ar ions, an ion beam current of 100 nA and a raster of 3×3 mm^2).

9. After sputtering, the Ar was pumped down and the Ti sublimation pump was switched on for a few seconds. After approximately 1 minute the pressure was $< 2 \times 10^{-8}$ Torr, and the linear segregation measurements were started.

Steps 6 to 9 were repeated for each segregation profile.

In the next chapter the experimental data obtained, using this first of a kind setup, are discussed. The data consists of three segregation profiles, which were ramped linearly at three different rates.

Chapter 6

Experimental Results and Discussion

6.1   Introduction

The results in this chapter are obtained from a novel experimental setup, where the electron beam is deflected from one surface (111) to the other (110) on a Cu bi-crystal, measuring the Sb segregation as the temperature is ramped linearly with time. This Positive Linear Heating technique (with deflecting electron beam) makes it possible to extract the segregation parameters for two different surfaces, accurately, from one segregation run. This ensures that all variables (i.e. temperature and pressure) are the same for the two surfaces during the segregation measurements and therefore the segregation parameters for these surfaces can be compared directly. In this chapter, experimental results are presented and discussed, that confirms the theory presented in **chapter 3** that states that the surface orientation of a crystal influences the bulk diffusion coefficient.

The AES data are processed in the following manner:

1. The noise is subtracted from the spectra, by taking the point with the lowest APPH (in the region where the Sb concentration is zero on the surface of the crystal, < 600 K) and subtracting that value from all the points in the spectrum.

2. The AES data is quantified by using previous LEED results [27, 28] to determine the maximum surface coverage.

3. The kinetic part of the segregation profile is fit with the Fick integral equation to extract the pre-exponential factor (D_0) and the activation energy (Q) as starting parameters for the Darken fits.

4. The equilibrium part of the segregation profile is fit with the Bragg-Williams equation to extract the segregation energy (ΔG) and the interaction energy (Ω_{CuSb}) as starting parameters for the Darken fits.

5. The segregation data is then fit with the Modified Darken Model, where the pre-exponential factor (D_0), the activation energy ($Q = Q_m + Q_v$), the segregation energy (ΔG) and the interaction energy (Ω_{CuSb}) is extracted. The error in the extracted values is calculated statistically.

The results presented in this chapter are also discussed in the following manner:

1. The difference in the activation energies between the two different surfaces (the (111) surface and the (110) surface) are discussed and compared to the theoretical absolute difference.

2. The pre-exponential factor is derived to show that the change in entropy is the reason for the difference in the pre-exponential factor values between the two surfaces. The difference in the change in entropy ($\Delta S_{\Delta s}$) between the (111) surface and the (110) surface is also calculated.

3. The interaction energies from the two different surfaces are discussed.

4. The segregation energy from the two different surfaces are discussed, and

5. the segregation parameters are compared to published results.

The same procedure was used to get a good statistical Modified Darken fit with the experimental data, for all the segregation profiles.

The 0.05 K.s^{-1} segregation run was the first segregation run and is seen as a test run. Unfortunately there were contaminants (S and C) present during the segregation run (see **figures 6.2**). This can be clearly seen in the steep decrease in the equilibrium concentration of Sb as a function of temperature. When the Sb reaches a maximum surface coverage the

contaminants starts to displace the Sb from the surface. Therefore the extracted segregation parameters from these two profiles (**figure 6.1**) are not used as part of the experimental confirmation for the theory discussed in **chapter 3**, or any discussions to follow

Figure 6.1: Measured Sb segregation in (A) Cu(110) and (B) Cu(111) for a linear temperature ramping run at a constant heating rate of 0.05 K.s^{-1}. The Modified Darken Model fit was done with the following parameters: (A) $D_0 = 7 \times 10^{-4}$ m^2.s^{-1}, $Q = 213$ kJ.mol^{-1}, $\Delta G = -86$ kJ.mol^{-1} and $\Omega_{CuSb} = -5$ kJ.mol^{-1}. (B) $D_0 = 1 \times 10^{-3}$ m^2.s^{-1}, $Q = 226$ kJ.mol^{-1}, $\Delta G = -80$ kJ.mol^{-1} and $\Omega_{CuSb} = 7$ kJ.mol^{-1}.
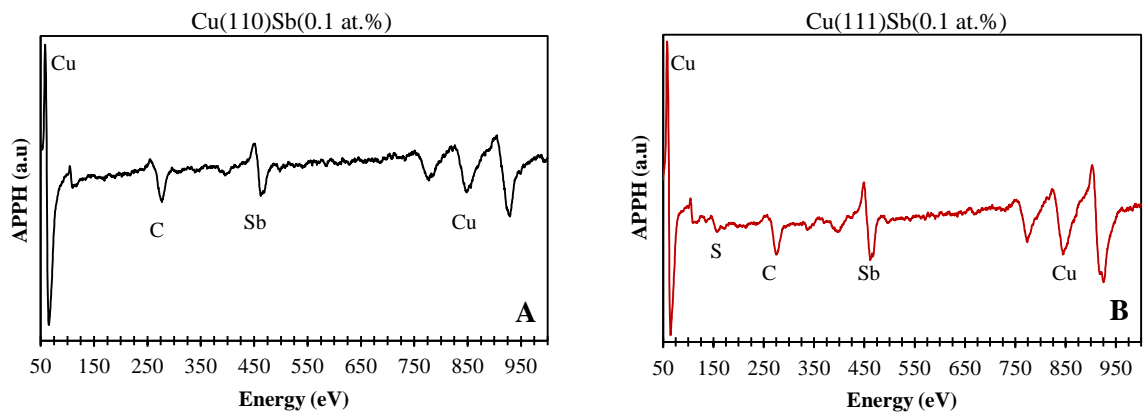
Figure 6.2: Measured Auger spectra of the (A) (110) surface and the (B) (111) surface after the linear temperature ramping run at a constant heating rate of 0.05 K.s^{-1} was completed.

From this test run it can be seen that there is a definite difference, in the measured segregation profiles, from the two surfaces.

6.2   Quantification

The measured Auger peak-to-peak height (APPH) in the derivative mode was quantified according to the following method.

It is based on Low Energy Electron Diffraction (LEED) patterns. A LEED photo of the cleaned samples is taken at room temperature before a run and shows only the atomic patterns of the substrate. After a run, the sample structure would be different as a result of segregation of the solute atoms from the bulk, and LEED photographs are taken again. The over layer structure can then be classified in terms of the substrate structure by the so called Wood's notation [27, 51, 67 − 72].

From the literature the maximum Sb fractional surface coverage in Cu(110) is 0.5 and in the Cu(111) 0.333.

6.3   The Fick Integral Fit

The low temperature region of the segregation profile is not sensitive to the segregation energy (ΔG) and interaction energy (Ω_{CuSb}). Roos et. al. [73] suggested a good fit is possible if the high temperature limit (T_E) is selected at a temperature where the coverage on the surface is approximately 10% of the maximum coverage (given that the segregation and interaction energies are relatively high). The high temperature limit for this study was selected at the temperature where the coverage is approximately 35% of the maximum coverage and the minimum temperature limit where the coverage is approximately 3%. This was done as the number of data points acquired from one orientation, up to a surface coverage of 10% of the maximum surface coverage, is too little and the interaction energy is much lower than the interaction energy suggested by Roos et. al. [73]. This temperature

88

region can thus be simulated using Fick's semi-infinite diffusion model. This method is used on all spectra (see **figure 6.3**).

The kinetic parameters, D_0 and Q (summarized in **table 6.1**), extracted with the Fick model are used as starting parameters for the Modified Darken Model.
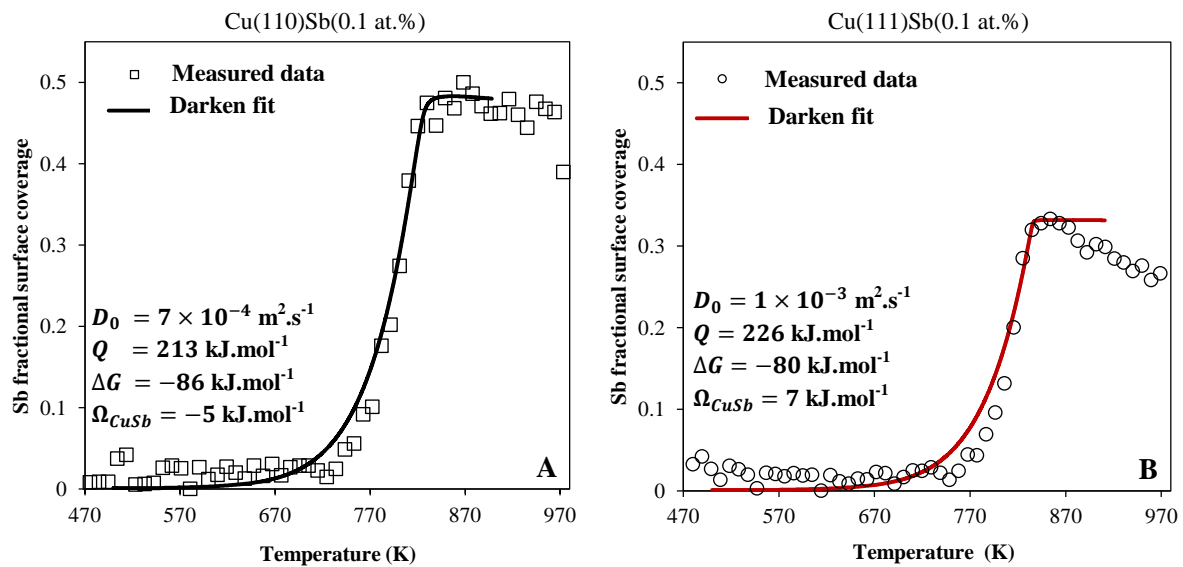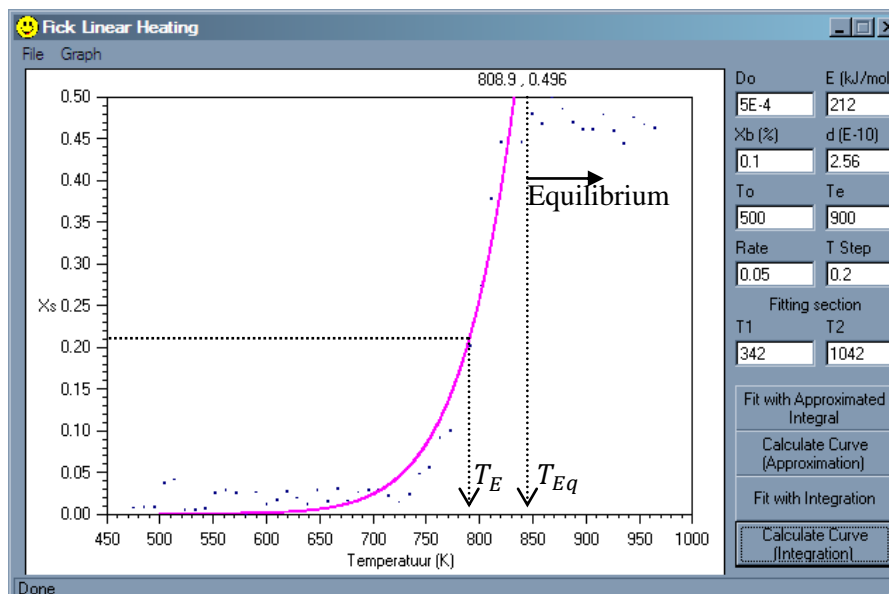

Figure 6.3: Measured Sb segregation in Cu(110) for a linear temperature ramping run at a constant heating rate of 0.05 K.s^{-1} and the calculated Fick integral with $D_0 = 5 \times 10^{-4}$ m^2.s^{-1} and $Q = 212$ kJ.mol^{-1}.

Orientation	Rate (K.s^{-1})	D_0 (m^2.s^{-1})	Q (kJ.mol^{-1})
Cu(110)	0.075	2.5×10^{-5}	198
	0.1	2.0×10^{-5}	194
Cu(111)	0.075	6.0×10^{-4}	232
	0.1	8.0×10^{-4}	232

Table 6.1: This table shows the extracted D_0 and Q values from the Fick model.

Temperatures above the chosen equilibrium temperature (T_{Eq}), showed by the dotted line, indicate the equilibrium segregation part of the profile that is fitted with the Bragg-Williams model.

6.4   The Bragg-Williams Fit

It is not easy to define where equilibrium segregation starts, therefore a temperature (T_{Eq}) for each profile is chosen where it seems (by inspection) as if the Sb surface coverage has started to reach an equilibrium point (see **figure 6.3**). A good statistical fit with the simulation is then determined. Again the segregation energies (ΔG) and the interaction energies (Ω_{CuSb}) were extracted with the Bragg-Williams equation and used as starting parameters for the Modified Darken Model (see **figure 6.4** and **Table 6.2**).
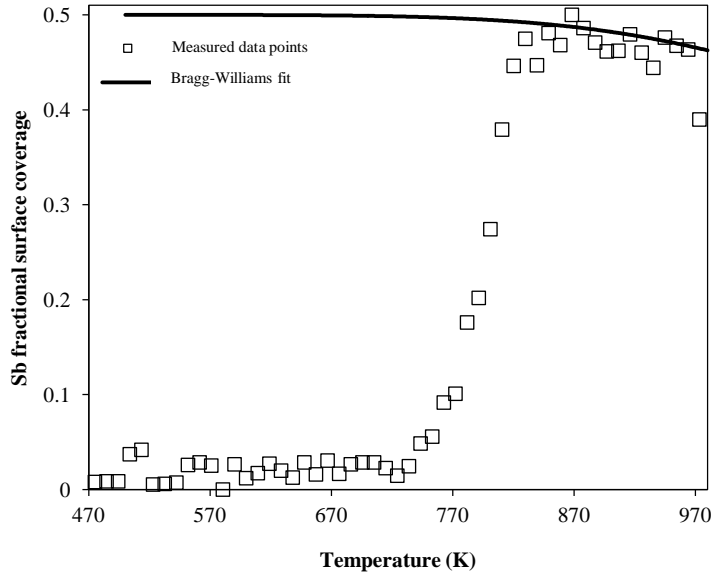
Figure 6.4: Measured Sb segregation in Cu(110) showing the equilibrium segregation profile fit, simulated with Bragg-Williams for $\Delta G = -86$ kJ.mol^{-1} and $\Omega_{CuSb} = -5$ kJ.mol^{-1}.

Orientation	Rate (K.s^{-1})	ΔG (kJ.mol^{-1})	Ω_{CuSb} (kJ.mol^{-1})
Cu(110)	0.075	-90 ± 1	-5 ± 1
	0.1	-90 ± 1	-5 ± 1
Cu(111)	0.075	-89 ± 1	-3 ± 1
	0.1	-88 ± 1	-3 ± 1

Table 6.2: This table shows the extracted ΔG and Ω_{CuSb} values from the Bragg-Williams model.

The segregation parameters D_0, Q, ΔG and Ω_{CuSb} obtained from the Fick integral and the Bragg-Williams equations are used as starting values for the Modified Darken Model.

91

6.5 The Modified Darken Fit

With the starting values obtained from the Fick and Bragg-Williams fits, a statistical good fit was determined with the Modified Darken Model. **Figures 6.5** to **6.6** show the measured segregation profiles at different heating rates and their corresponding Modified Darken fits. The extracted segregation parameters (D_0, Q, ΔG and Ω_{CuSb}) are summarized in **table 6.3**.

Figure 6.5 show the measured segregation profiles in the Cu(110/111) bi-crystal, at a constant heating rate of 0.075 K.s^{-1}.

Cu(110)Sb(0.1 at.%)　　　　　　Cu(111)Sb(0.1 at.%)

$D_0 = 2.3 \times 10^{-5}$ m^2.s^{-1}
$Q = 197$ kJ.mol^{-1}
$\Delta G = -90$ kJ.mol^{-1}
$\Omega_{CuSb} = -5$ kJ.mol^{-1}

$D_0 = 1.1 \times 10^{-3}$ m^2.s^{-1}
$Q = 233$ kJ.mol^{-1}
$\Delta G = -89$ kJ.mol^{-1}
$\Omega_{CuSb} = -3$ kJ.mol^{-1}

Figure 6.5: Measured Sb segregation in (A) Cu(110) and (B) Cu(111) for a linear temperature ramping run at a constant heating rate of 0.075 K.s^{-1}. The Modified Darken Model fit was done with the following parameters: (A) $D_0 = 2.3 \times 10^{-5}$ m^2.s^{-1}, $Q = 197$ kJ.mol^{-1}, $\Delta G = -90$ kJ.mol^{-1} and $\Omega_{CuSb} = -5$ kJ.mol^{-1} and (B) $D_0 = 1.1 \times 10^{-3}$ m^2.s^{-1}, $Q = 233$ kJ.mol^{-1}, $\Delta G = -89$ kJ.mol^{-1} and $\Omega_{CuSb} = -3$ kJ.mol^{-1}.

Figure 6.6 show the measured segregation profiles in the Cu(110/111) bi-crystal, at a constant heating rate of 0.1 K.s^{-1}.
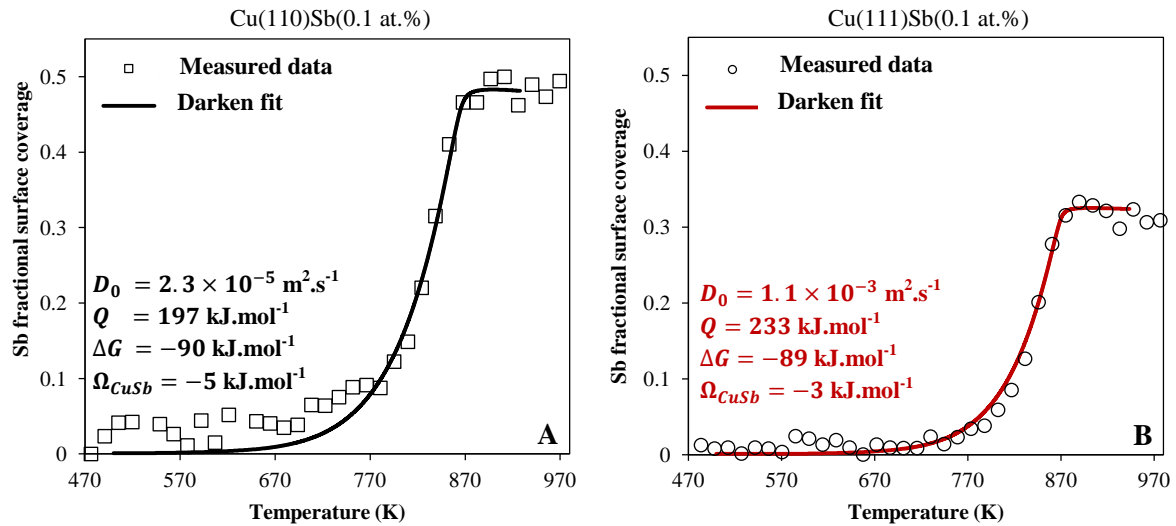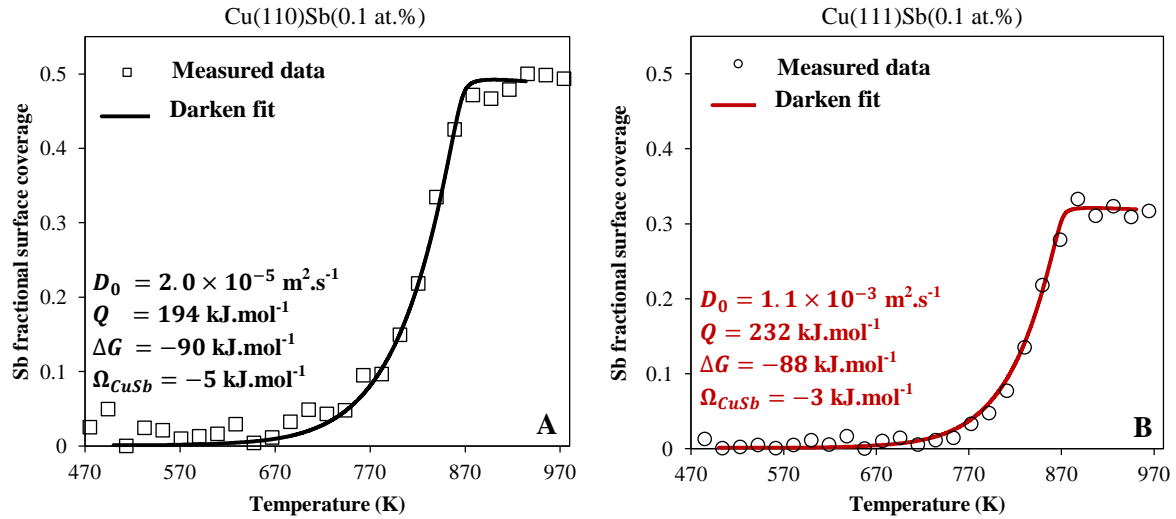

Figure 6.6: Measured Sb segregation in (A) Cu(110) and (B) Cu(111) for a linear temperature ramping run at a constant heating rate of 0.1 K.s^{-1}. The Modified Darken Model fit was done with the following parameters: (A) $D_0 = 2.0 \times 10^{-5}$ m^2.s^{-1}, $Q = 194$ kJ.mol^{-1}, $\Delta G = -90$ kJ.mol^{-1} and $\Omega_{CuSb} = -5$ kJ.mol^{-1} and (B) $D_0 = 1.1 \times 10^{-3}$ m^2.s^{-1}, $Q = 232$ kJ.mol^{-1}, $\Delta G = -88$ kJ.mol^{-1} and $\Omega_{CuSb} = -3$ kJ.mol^{-1}.

Orientation	Rate (K.s^{-1})	D_0 (m^2.s^{-1}) ($\pm 5\%$)	Q (kJ.mol^{-1})	ΔG (kJ.mol^{-1})	Ω_{CuSb} (kJ.mol^{-1})
Cu(110)	0.075	2.3×10^{-5}	197 ± 2	-90 ± 1	-5 ± 1
	0.1	2.0×10^{-5}	194 ± 2	-90 ± 1	-5 ± 1
Cu(111)	0.075	1.1×10^{-3}	233 ± 2	-89 ± 1	-3 ± 1
	0.1	1.1×10^{-3}	232 ± 2	-88 ± 1	-3 ± 1

Table 6.3: The segregation parameters experimentally extracted from the Darken model in the Cu(110)/(111)Sb(0.1 at.%) bi-crystal.

By comparing the activation energies (Q) of the two different surfaces, it is evident that the activation energy under the (111) surface is approximately 18% higher than the activation energy under the (110) surface. Also, comparing the pre-exponential factor (D_0) under the two different surfaces, there is an average difference of 1.1×10^{-3} m^2.s^{-1}. The segregation energy (ΔG) has an average value of -90 kJ.mol^{-1}. The interaction energy (Ω_{CuSb}) for the Cu(110) surface is -5 kJ.mol^{-1} and -3 kJ.mol^{-1} for the Cu(111) surface.

In the following paragraphs the results are discussed for the (110) and the (111) surface, where the difference in the activation energy, the difference in the pre-exponential factor and the difference in the interaction energy will be discussed.

6.6   The Activation Energy(Q)

It was proposed by J. J. Terblans et al. [27, 29, 47, 74, 75] that the bulk diffusion coefficient obtained in surface segregation measurements is surface orientation dependent because the surface properties influence the vacancy concentration.

In **chapter 3**, the bulk diffusion coefficient (D) is rewritten by expanding the activation energy (Q) into two terms: (i) the migration energy (E_m), the minimum energy that an atom needs to move in the bulk and, (ii) the vacancy formation energy (E_v), the energy needed to form a vacancy. According to this theory, E_v is dependent on the difference between the number of nearest neighbours (bonds) an atom in the surface have and an atom in the bulk have. E_v under the (111) surface is approximately 29% higher than that under the (110) surface. As reported in **chapter 3,** calculations done by Terblans [27], shows the difference in the activation energy (Q) under the (110) surface and the (111) surface is approximately 17%.

Terblans et. al. [29] tried to measure this difference on two single crystals, a Cu(111)Sb(0.082 at. %) and a Cu(110)Sb(0.087 at. %). It is reported that the activation energy for the Cu(111)Sb(0.082 at. %) crystal is 18 % higher than the activation energy for the Cu(110)Sb(0.087 at. %) crystal.

These crystals had different impurity concentrations (i.e. Sb). A difference in the true heating rate (α) cannot be ruled out for the two crystals [30]. Also, these measurements were done at different times and therefore the segregation in the two single crystals was measured at different vacuum pressures and at different room temperatures that influence the electronics of the AES system. In the present study the segregation in a Cu bi-crystal was measured, ruling out all these differences.

Figure 6.7 shows the measured segregation profiles in the Cu(111/110) bi-crystal, at a constant heating rate of 0.075 K.s^{-1}.

Figure 6.7: Measured Sb segregation in (A) Cu(110) and (B) Cu(111) for a linear temperature ramping run at a constant heating rate of 0.075 K.s⁻¹. The Modified Darken Model fit was done with the following parameters: (A) $D_0 = 2.3 \times 10^{-5}$ m².s⁻¹, $Q = 197$ kJ.mol⁻¹, $\Delta G = -90$ kJ.mol⁻¹ and $\Omega_{CuSb} = -5$ kJ.mol⁻¹ and (B) $D_0 = 1.1 \times 10^{-3}$ m².s⁻¹, $Q = 233$ kJ.mol⁻¹, $\Delta G = -89$ kJ.mol⁻¹ and $\Omega_{CuSb} = -3$ kJ.mol⁻¹.

Orientation	Rate (K.s⁻¹)	Q (kJ.mol⁻¹)	Percentage Difference
Cu(110)	0.075	197 ± 2	**16.7** %
Cu(111)	0.075	233 ± 2	

Table 6.4: The activation energies experimentally extracted from the Sb segregation profiles with a temperature ramping constant of 0.075 K.s⁻¹ and the percentage difference between the two.

The activation energy (Q) for the (111) surface is 197 kJ.mol^{-1} and for the (110) surface it is 233 kJ.mol^{-1}. It is calculated that the activation energy under the (111) surface is approximately 17% higher than that under the (110) surface.

Figure 6.8 shows the measured segregation profiles in the Cu(110/111) bi-crystal, at a constant heating rate of 0.1 K.s^{-1}
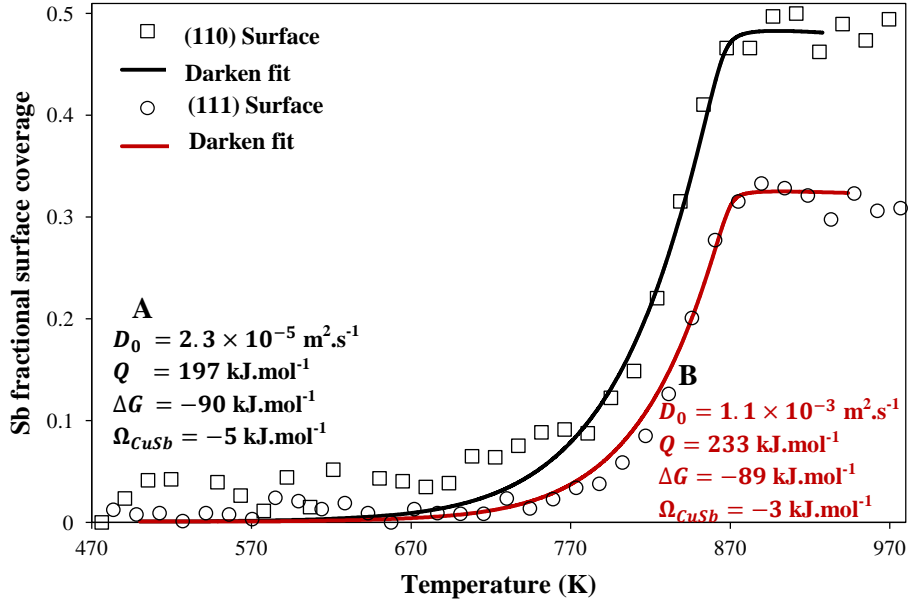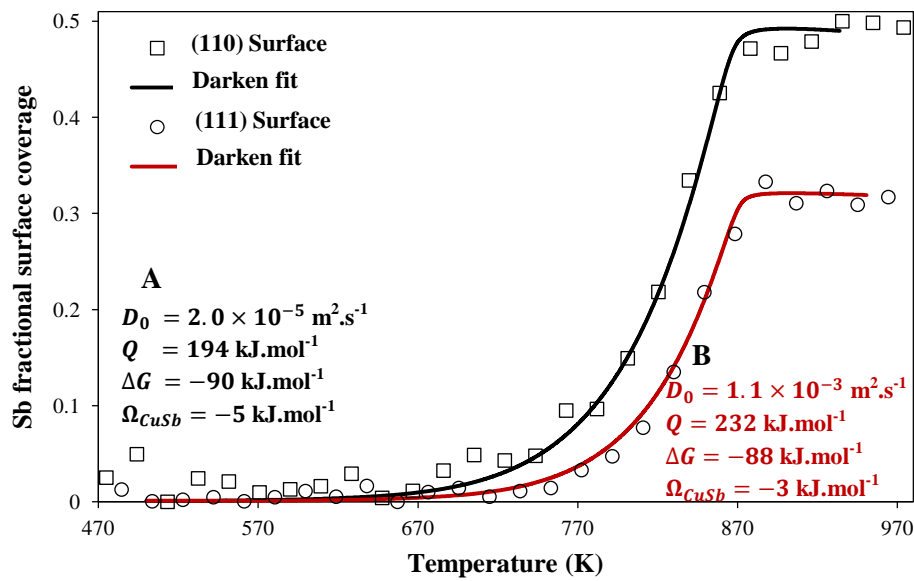

Figure 6.8: Measured Sb segregation in (A) Cu(110) and (B) Cu(111) for a linear temperature ramping run at a constant heating rate of 0.1 K.s^{-1}. The Modified Darken Model fit was done with the following parameters: (A) $D_0 = 2.0 \times 10^{-5}$ m².s[-1], $Q = 194$ kJ.mol^{-1}, $\Delta G = -90$ kJ.mol^{-1} and $\Omega_{CuSb} = -5$ kJ.mol^{-1} and (B) $D_0 = 1.1 \times 10^{-3}$ m².s[-1], $Q = 232$ kJ.mol^{-1}, $\Delta G = -88$ kJ.mol^{-1} and $\Omega_{CuSb} = -3$ kJ.mol^{-1}.

Orientation	Rate $(K.s^{-1})$	Q $(kJ.mol^{-1})$	Percentage Difference
Cu(111)	0.1	194 ± 2	
Cu(110)	0.1	232 ± 2	**17.8** %

Table 6.5: The activation energies experimentally extracted from the Sb segregation profiles with a temperature ramping constant of 0.1 K.s^{-1} and the percentage difference between the two.

The activation energy (Q) for the (111) surface is 194 kJ.mol^{-1} and for the (110) surface it is 232 kJ.mol^{-1}. It is calculated that the activation energy under the (111) surface is approximately 18% higher than that under the (110) surface.

Orientation	Rate $(K.s^{-1})$	Q $(kJ.mol^{-1})$	Average Percentage Difference
Cu(111)	0.075	197 ± 2	
	0.1	194 ± 2	
Cu(110)	0.075	233 ± 2	**17.2** %
	0.1	232 ± 2	

Table 6.6: The activation energies experimentally extracted from the Sb segregation profiles and the average percentage difference between the activation energies of the two surfaces.

From the experimental data (see **figures 6.7** and **6.8**) it is evident that the Sb segregation to the (110) surface is faster than the Sb segregation to the (111) surface. This is because the average activation energy for diffusion under the (111) surface is approximately 17% higher than under the (110) surface. This difference is comparable to the 17% that is predicted by the theoretical model, thus confirming the theory that the surface orientation influences the

bulk diffusion coefficient. Also, these results obtained from this study, is in good agreement with the 18% difference Terblans [27, 29] obtained experimentally.

6.7   The Pre-exponential Factor (D_0)

From the extracted D_0 values in **table 6.7** (see **figures 6.7** and **6.8**) it is apparent that the pre-exponential factor under the (111) surface differ from the pre-exponential factor under the (110) surface.

Orientation	Rate (K.s^{-1})	D_0 (m^2.s^{-1}) ($\pm 5\%$)	Average D_0 (m^2.s^{-1})
Cu(110)	0.075	2.3×10^{-5}	2.2×10^{-5}
	0.1	2.0×10^{-5}	
Cu(111)	0.075	1.1×10^{-3}	1.1×10^{-3}
	0.1	1.1×10^{-3}	

Table 6.7:   The pre-exponential factors experimentally extracted from the Sb segregation profiles.

It is shown that the diffusion coefficient can be written as [76]:

$$D_A = f_c \frac{\Gamma_A d^2}{6} = f_c \frac{\rho \gamma_A d^2}{6}$$
(6.1)

where f_c is the correlation factor ($f_c \leq 1$), ρ the probability factor, γ_A the atomic jump frequency and d the jump distance.

For vacancy diffusion ρ is equal to the probability that there is a neighbouring defect available to mediate the jump.

The temperature dependence arises from two distinct thermodynamic factors:

1. The vacancy formation term (E_v), (it cost thermal energy to create the defects).

2. The atomic migration term (E_m), (it cost thermal energy to transfer an atom from one site to another).

The Gibbs free energy of formation of a vacancy is:

$$\Delta g_v = \Delta h_v - T\Delta s_v \qquad (6.2)$$

where Δh_v is the change in enthalpy, T the temperature and Δs_v the change in vacancy formation entropy.

The fraction of vacancies in thermal equilibrium is thus given by:

$$x_v = e^{-\Delta g_v/k_B T}, \qquad (6.3)$$

Thus the probability of finding a vacancy is:

$$\rho = e^{-\Delta g_v/k_B T} \qquad (6.4)$$

The migration free energy (free energy difference between the activated and the initial configurations) is given by:

$$\Delta g_m = \Delta h_m - T\Delta s_m \qquad (6.5)$$

The probability of having sufficient energy to surmount the energy barrier occur with a frequency proportional to the Boltzmann factor:

$$e^{-\Delta g_m/k_B T}$$

The jump frequency of the atom (γ_A) is now equal to the product of the atomic vibrational frequency v_A and the probability of executing a jump:

$$e^{-\Delta g_m/k_B T}$$

$$\gamma_A = v_A e^{-\Delta g_m/k_B T} \tag{6.6}$$

and therefore,

$$
\begin{aligned}
D &= f_c \frac{\Gamma_A d^2}{6} = f_c \frac{\rho \gamma_A d^2}{6} \\
&= f_c \frac{d^2}{6} e^{-\Delta g_v/k_B T} v_A \, e^{-\Delta g_m/k_B T} \\
&= v_A f_c \frac{d^2}{6} e^{-(\Delta h_v - T\Delta s_v)/k_B T} e^{-(\Delta h_m - T\Delta s_m)/k_B T} \\
&= v_A f_c \frac{d^2}{6} e^{(\Delta s_m + \Delta s_v)/k_B} e^{-(\Delta h_v + \Delta h_m)/k_B T}
\end{aligned}
$$

$$\tag{6.7}$$

with

$$D_0 = v_A f_c \frac{d^2}{6} e^{(\Delta s_m + \Delta s_v)/k_B} \tag{6.8}$$

that is also known as the pre-exponential factor, which is temperature independent and

$$Q = \Delta h_v + \Delta h_m \tag{6.9}$$

also known as the activation energy.

From the derivation above (see **equation 6.8**), it is clear that D_0 is a function of the change in entropy ($\Delta s_m + \Delta s_v$), which includes the terms for, (i) the change in entropy for the migration

101

of an atom in the bulk (Δs_m) and (ii) the change in entropy for vacancy formation (Δs_v). The change in entropy for the migration of an atom in the bulk is assumed to be the same for the (111) surface and the (110) surface. The change in entropy for vacancy formation, on the contrary, is different for the two surfaces. This is because the number of vacancies under the two surfaces differs and therefore, the degrees of disorder for the two surfaces differ. This results in a pre-exponential factor ($D_0^{(111)}$) for the (111) surface that differs from the pre-exponential factor ($D_0^{(110)}$) for the (110) surface (see **table 6.7**).

From this difference in the pre-exponential factors of the (111) surface and the (110) surface, it is then possible to calculate the difference in the change in entropy ($\Delta S_{\Delta s}$) between the two surfaces.

From **equation 6.8** the D_0 for each surface can be written as:

$$D_0^{(111)} = \nu_A f_c \frac{d_{(111)}^2}{6} e^{(\Delta s_m + \Delta s_v^{(111)})/k_B} \tag{7.10}$$

$$D_0^{(110)} = \nu_A f_c \frac{d_{(110)}^2}{6} e^{(\Delta s_m + \Delta s_v^{(110)})/k_B} \tag{7.11}$$

where the atomic vibrational frequency ν_A is constant for both surface orientations, and the correlation factor f_c is constant for a specific diffusion mechanism (vacancy diffusion mechanism in the case of Sb in a Cu matrix). **Equations 6.10** and **6.11** can now be written in the form:

$$D_0^{(111)} = K d_{(111)}^2 e^{(\Delta s_m + \Delta s_v^{(111)})/k_B} \tag{7.12}$$

$$D_0^{(110)} = K d_{(110)}^2 e^{(\Delta s_m + \Delta s_v^{(110)})/k_B} \tag{7.13}$$

Dividing **equation 6.12** in **6.13** gives:

$$\frac{D_0^{(111)}}{D_0^{(110)}} = \frac{d_{(111)}^2}{d_{(110)}^2} e^{\left(\frac{\Delta s_m}{k_B} + \frac{\Delta s_v^{(111)}}{k_B}\right) - \left(\frac{\Delta s_m}{k_B} + \frac{\Delta s_v^{(110)}}{k_B}\right)} \tag{7.14}$$

$$\frac{D_0^{(111)}}{D_0^{(110)}} = \frac{d_{(111)}^2}{d_{(110)}^2} e^{\left(\frac{\Delta s_v^{(111)} - \Delta s_v^{(110)}}{k_B}\right)} \tag{7.15}$$

$$\ln \frac{D_0^{(111)}}{D_0^{(110)}} = \ln \frac{d_{(111)}^2}{d_{(110)}^2} + \left(\frac{\Delta s_v^{(111)} - \Delta s_v^{(110)}}{k_B}\right) \tag{7.16}$$

$$\ln x_1 - \ln x_2 = \left(\frac{\Delta s_v^{(111)} - \Delta s_v^{(110)}}{k_B}\right) \tag{7.17}$$

where $x_1 = \frac{D_0^{(111)}}{D_0^{(110)}}$ and $x_2 = \frac{d_{(111)}^2}{d_{(110)}^2}$

$$\Delta S_{\Delta s} = \Delta s_v^{(111)} - \Delta s_v^{(110)} = k_B [\ln x_1 - \ln x_2] \tag{7.18}$$

where $\Delta s_v^{(111)} - \Delta s_v^{(110)}$ is the difference in the change in entropy ($\Delta S_{\Delta s}$).

Thus the change in the change in entropy between the (111) surface and the (110) surface is:

$$\Delta S_{\Delta s} = 8.31 \text{ J. mol}^{-1}\text{K}^{-1} \times \left[\ln 50 - \ln \frac{2}{3}\right]$$

$$= 36 \text{ J.mol}^{-1}\text{K}^{-1}$$

Due to the fact that there is a difference in the change in entropy between the two surfaces, there must be a difference in the pre-exponential factors if the surface orientations differ.

6.8   The Interaction of Sb with Cu (Ω_{CuSb})

For ideal solutions Ω is zero, and there are no additional interactions between the species that constitutes the solution. In terms of nearest neighbour interactions only, the energy of an $A - B$ interaction, μ_{AB}, equals the average of the $A - A$, μ_{AA}, and $B - B$, μ_{BB}, interactions or

$$\Omega = zN \left[\mu_{AB} - \frac{(\mu_{AA} + \mu_{BB})}{2} \right] \tag{6.19}$$

where z is the coordination number and N Avogardo's number [77]. For the general case, as in this study, of a non ideal solution $\Omega < 0$ gives an increased stability of the solution relative to an ideal solution, while $\Omega > 0$ destabilizes the solution. It follows that $\Omega < 0$ and $\Omega > 0$ are interpreted as attractive and repulsive interactions, respectively, between the A and B atoms.

Researches [27, 28, 51] that are concerned with segregation tend to make the assumption that the interaction parameter is zero ($\Omega = 0$). However, Asante et. al. [78] extracted the interaction parameters, for the first time, from a ternary system (CuSnSb). Asante et. Al. Obtained interaction parameters for the interaction of Sb with Cu(111) and Sb with Cu(110) as 16.2 kJ.mol^{-1} and 15.9 kJ.mol^{-1}, respectively.

In the table below are interaction parameters extracted in this study from a CuSb binary system.

Orientation	Rate (K.s^{-1})	Ω_{CuSb} (kJ.mol^{-1})
Cu(110)	0.075	-5 ± 1
	0.1	-5 ± 1
Cu(111)	0.075	-3 ± 1
	0.1	-3 ± 1

Table 6.8: The interaction parameters experimentally extracted from the Cu(110)/(111)Sb(0.1 at.%) bi-crystal.

Asante et. al. obtained relatively high positive values for the interaction parameters, although he defined the positive, also as an attractive interaction (the negative value from the present work is defined as an attractive interaction).

6.8.1 The Interaction Parameters from Two Different Orientations

From the definition above (see **equation 6.19**) one can see that the interaction parameter (Ω) is a function of an atom's nearest neighbours (number of bonds with the atom). In the different surfaces, therefore, the interaction parameters would be different. This is because, as discussed in **chapter 3**, the number of bonds with an adatom in the (111) surface is 3 and in the (110) surface it is 5. This results in a interaction parameters from the (111) surface that differs from the interaction parameter from the (110) surface (see **table 6.8**).

6.9 The Segregation Energy (ΔG)

The segregation energy, which is negative values, is responsible for the enrichment of the surface layer by the segregating element. The difference in standard chemical potentials, of

the matrix atoms and the solvent atoms in the bulk and in the surface is the segregation energy (ΔG), as discussed in **chapter 2.**

Orientation	Rate (K.s^{-1})	ΔG (kJ.mol^{-1})	Average ΔG (kJ.mol^{-1})
Cu(110)	0.075	-90 ± 1	-90
	0.1	-90 ± 1	
Cu(111)	0.075	-89 ± 1	-89
	0.1	-88 ± 1	

Table 6.9: The segregation energies experimentally extracted from the Cu(110)/(111)Sb(0.1 at.%) bi-crystal.

6.10 Comparing Extracted Segregation Parameters
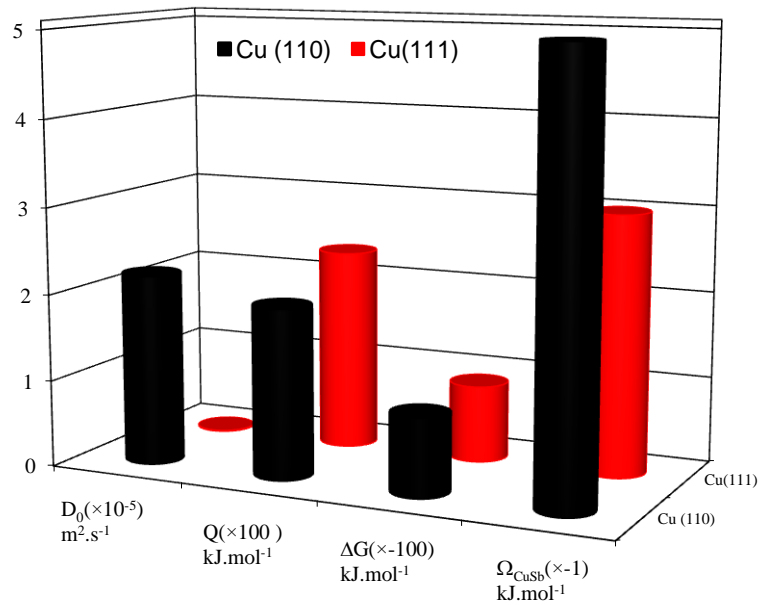

Figure 6.9: Comparing the extracted segregation parameters.

Orientation	D_0 (m^2.s^{-1})	Q (kJ.mol^{-1})	ΔG (kJ.mol^{-1})	Ω_{CuSb} (kJ.mol^{-1})	Reference

	2.2×10^{-5}	196	-90	-5	Present work
Cu(110)	1.1×10^{-6}	155	-80	$-$	[27]
	3.3×10^{-6}	170	-71	$-$	[51]
Cu(111)	1.1×10^{-3}	233	-89	-3	Present work
	4.3×10^{-5}	183	-82	$-$	[27]
	2.8×10^{-5}	201	-77	$-$	[51]

Table 6.10: Published results compared to the results obtained from this study.

It is clear from **table 6.10** that segregation parameters of Sb obtained for the present study compare fairly well with other published results. The difference in the segregation parameters can be attributed to the fact that the effective Sb bulk concentration in the grains of the Cu bi-crystal is actually lower than what was determined due to localized energy pits in the grain boundary [79].

6.11 Summary

- The AES system has been modified successfully in order to deflect the e⁻ beam from one surface to the other, of the bi-crystal.

- A new program has also been developed in order to automate the deflection of the e⁻ beam and the segregation data acquisition process.

- The percentage difference in the activation energy obtained from this experimental segregation results is approximately 17%, which is in good agreement with other published results.

- The experimental results obtained with this one of a kind experimental setup confirm the theory discussed in **chapter 3.**

- In this study it is found that there is a difference in the pre-exponential factors (D_0) from the two different surface orientations where $D_0^{(110)} = 2.2 \times 10^{-5}$ m^2.s^{-1} and $D_0^{(111)} = 1.1 \times 10^{-3}$ m^2.s^{-1}. By rewriting the pre-exponential factor in a more extended form it is seen that the pre-exponential factor is a function of the change in entropy. This term consists of the change in entropy for the migration of an atom in the bulk term (Δs_m) and the change in entropy for vacancy formation term (Δs_v). Therefore the difference in the change in entropy ($\Delta S_{\Delta s}$) is calculated as 36 J.mol^{-1}K^{-1}.

- The extracted interaction parameter for the Cu(110) differ from the one of the Cu(111). The interaction parameters are determined to be $\Omega_{CuSb}^{(110)} = -5$ kJ.mol^{-1} and $\Omega_{CuSb}^{(110)} = -3$ kJ.mol^{-1}. The difference is attributed to (i) the fact that an adatom on the two different surface orientations have different number of bonds, and (ii) the difference in the change in entropy of the two different surface orientations.

- The segregation energies from the two different surfaces are $\Delta G^{(110)} = -90$ kJ.mol^{-1} and $\Delta G^{(111)} = -89$ kJ.mol^{-1}.

6.12   Suggested Future Work

1. The grain boundary in the bi-crystal can be seen as an energy pit where impurity atoms get trapped. These trapped impurities do not contribute to the effective impurity concentration in the grains. It is thus suggested that the true contribution that the grain boundary has, in the reduction of the effective impurity concentration, be

investigated. This can be done by investigating segregation in polycrystalline samples involving the contribution of each surface orientation to the total surface of the crystal. When using polycrystalline samples for segregation, grain boundary segregation is an integral part of such a project. This can be done studying individual grains with a high resolution AES system.

2. Segregation is a well known phenomenon in this department and a lot of fundamental research has been done on this subject. It is thus suggested that the practical applications of segregation be investigated. Segregation can be applied in the catalytic research field to engineer self healing catalysts. It can also be applied in the material protection research field where segregation is used to form a protective layer (i.e. Al) and protect the material from corrosion. This can be useful in cathodes for Al smelters, where the Cu alloy cathode makes use of the Al on the cathode surface to protect it from corrosion.

3. Only AES has been used so far to extract segregation parameters by monitoring the changes in concentration build up on the surface while heating the sample linearly with time. It is suggested that the XPS (PHI 5400) in the Physics Department at the University of the Free State be modified in order to heat samples linearly during XPS measurements. This will allow the researcher to not only monitor the changes in surface concentration as the sample is heated linearly, but also the changes in the chemical state as the concentration on the surfaces changes.

Results from this Study Already Announced

1. CJ Jafta, WD Roos and JJ Terblans, *'n Gebruikersvriendelike uitgloeisisteem*, Suid Afrikaanse Tydskrif vir Natuurwetenskap en Tegnologie, **3** (2009) 249.

2. CJ Jafta, WD Roos, JJ Terblans and AB Hugo, A pressurized Ar-filled annealing system, Instrumentation Science and Technology, **4** (2010) 261

3. CJ Jafta, WD Roos, S Cronjé and JKO Asante, *Die invloed van Sb dotering op die korrelgroei van polikristallyne Cu*, Submitted for publication to the online journal LitNet November 2010.

Conference Contributions

1. CJ Jafta, JJ Terblans and WD Roos, An argon filled user – friendly annealing system, South African Institute of Physics (SAIP) 53rd Annual Conference at the University of Limpopo, (2008)

2. CJ Jafta, JJ Terblans and WD Roos, 'n Gebruikersvriendelike uitgloeisisteem, 8ste Suid Afrikaanse Akademie vir Wetenskap en Kuns (SAAWK) Simposium at the University of Johannesburg, (2008)

3. CJ Jafta, JKO Asante, S Cronjé and WD Roos, Influence of Sb doping on grain growth of polycrystalline Cu, South African Institute of Physics (SAIP) 55th Annual Conference at the CSIR International Convention Centre, Pretoria, (2010)

REFERENCES

1. P.A. Dowben and A. Miller, *Surface Segregation Phenomena,* CRC Press, (1990).

2. M. Ashby, H. Shercliff and D. Cebon, *Materials Engineering, Science, Processing and Design,* Elsevier, (2007).

3. R.S. Graves and R.R. Zarr, *Insulation Materials, Testing and Applications,* 4th Volume, ASTM International, (1997).

4. J. Qin, D. He, L. Lei, P. An, L. Fang, Y. Li, F. Wang and Z. Kou, Journal of Alloys and Compounds, **476,** (2009), L8.

5. C.J. Jafta, W.D. Roos, S. Cronjè and J.K.O. Asante, Manuscript submitted to the online Journal LitNet for publication, November 2010.

6. T.D. Lee, M.S. Hwang and K.J. Lee, Journal of Magnetism and Magnetic Materials, **235**, (2001), 297.

7. S. Tsurekawa, K. Kawahara, K. Okamoto, T. Watanabe and R. Faulkner, Materials Science and Engineering A, **387,** (2004), 442.

8. M.A. Reijme, A.W. Denier van der Gon, M. Draxler, A. Gildenpfennig, F.J.J. Janssen and H.H. Brongersma, Surface and Interface Analysis, **36**, (2004), 1.

9. M. Batzill and U. Diebold, Progress in Surface Science, **79,** (2005), 47.

10. J.R. Jinschek, R. Erni, N.F. Gardner, A.Y. Kim and C. Kisielowski, Solid State Communications, **137,** (2006), 230.

11. M.P. Seah, Surface Science, **53,** (1975), 168.

12. F.M. d'Heurle and A. Gangulee, *The Nature and Behavior of Grain Boundaries*, H. Hu, Editor, Plenum Press, (1972).

13. D. Gupta, Metallurgical Transactions, **8A,** (1977), 1431.

14. W.C. Johnson and D.F. Stein, Journal of American Ceramic Society, **58,** (1975), 485.

15. B.S. Bokstein, C.V. Kopetzikii and L.S. Shvindlerman, *Thermodynamics and Kinetics of Grain Boundaries During Microstructural Evolution,* Colorado School of Mines, (2006).

16. L.S. Shvindlerman, G. Gottstein and D.A. Moldov, Physica Status Solidi, **160,** (1997), 419.

17. G. Gottstein and L.S. Shvindlerman, *Grain Boundary Migration in Metals – Thermodynamics, Kinetics, Applications,* 2nd Edition, Taylor and Francis, (2009).

18. R.M. Latanision and H. Opperhauser (jr.), Metallurgical Transactions, **5,** (1974), 483.

19. S. Dinda and W.R. Warke, Materials Science and Engineering, **24,** (1976), 199.

20. J.H. Sinfelt, Advanced Catalysis, **23,** (1973), 91.

21. C.R. Helm and J.H. Sinfelt, Surface Science, **72,** (1978), 229.

22. G. Gurdag and T. Hahn, Applied Catalysis A: General, **192,** (2000), 51.

23. J. du Plessis, *Diffusion and Defect Data B,* Sci – Tech Publications, **11** (1990).

24. P. Wynblatt and R.C. Ku, Surface Science, **65,** (1977), 511.

25. F.F. Abraham, Physics Review Letters, **46,** (1981), 546.

26. J.A. Barnard, P. Wynblatt, W.C. Johnson and W.W. Mullins, Surface Science, **183,** (1988), 363.

27. J.J. Terblans, Ph.D. Thesis, University of the Free State, South Africa (2001).

28. J.K.O. Asante, Ph.D. Thesis, University of the Free State, South Africa (2006).

29. J.J. Terblans and G.N. van Wyk, Surface and Interface Analysis, **36,** (2004), 935.

30. E.C. Viljoen and J. du Plessis, Surface Science, **468,** (2000), 27.

31. H. Mehrer, *Diffusion in Solids: Fundamentals, Methods, Materials, Diffusion-Controlled Processes,* M. Cardona, P. Fulde, K. von Klitzing and H. Queisser, Editors, Springer, (2007).

32. L.W. Barr, H. Mehrer, Chr. Herzig, N.A. Stolwijk and H. Bracht, DIMAT 96, **1,** (1997), 1.

33. J. Philibert, Diffusion Fundamentals, **2,** (2005), 1.1.

34. JN Sherwood, *Diffusion Processes: Proceedings of the Thomas Graham Memorial Symposium*, **1,** (1971).

35. A Fick, Philosophical Magazine S.4, **10,** (1855), 30.

36. S. Arrhenius, Zeitschrift für Physikalische Chemie, **4**, (1889), 226.

37. W.C. Roberts-Austen, Philosophical Transactions of the Royal Society of London Series A, **187,** (1896), 383.

38. A. Einstein, R. Fürth and A.D. Cowper, *Investigation on the Theory of the Brownian movement,* Dover Publications, (1956).

39. L.S. Darken, Trans. AIME, **180,** (1949), 430.

40. J. Crank, *The Mathematics of Diffusion,* 2nd Edition, Claredon Press, (1975).

41. C.H.P. Lupis, *Chemical Thermodynamics of Materials,* North – Holland, (1983).

42. J.H. Hildebrand and R.L. Scott, *The Solubility of Nonelectrolytes*, 3rd edition, Dover Publications, (1950).

43. H. Viefhaus and M. Rüsenberg, Surface Science, **159,** (1985), 1.

44. M.A. Omar, *Elementary Solid State Physics: Principles and Applications,* 1st edition, Addison-Wesley Publication Company, (1975).

45. M.E. Glicksman, *Diffusion in Solids: Field Theory, Solid State Principles, and Applications,* 1st edition, Wiley, (2000).

46. R.J. Borg and G.J. Dienes, *An Introduction to Solid State Diffusion,* 1st edition, Academic Press, (1988).

47. J.J. Terblans, W.J. Erasmus, E.C. Viljoen and J. du Plessis, Surface and Interface Analysis, **28,** (1999), 70.

48. M. Breeman, G.T. Barkema and D.O. Boerma, Surface Science, **323,** (1995), 71

49. E.C. Viljoen and J. du Plessis, Surface Science, **431,** (1999), 128.

50. C.P. Flynn, *Point Defects and Diffusion,* Clarendon Press, (1972).

51. W.J. Erasmus, M.Sc. Thesis, University of the Free State*,* South Africa (1999).

52. S. Divinski, M. Lohmann and Chr. Herzig, Acta materialia, **49,** (2001), 249.

53. K.D. Hobart, D.J. Godbey, M.E. Twigg, M. Fatemi, P.E. Thompson and D.S. Simons, Surface Science, **334,** (1995), 29.

54. W.T. Wu, R.Y. Yan, Y. Niu and F. Gesmundo, Corrosion Science, **39,** (1997), 1831.

55. G.Y. Fu, Y. Niu, W.T. Wu and F. Gesmundo, Corrosion Science, **40,** (1998), 1215.

56. Y. Niu, Y.S. Li and F. Gesmundo, Corrosion Science, **42,** (2000), 165.

57. G.J. Liu, S.S. Jia, Y.F. Zhu, S.H. Hong, J.W. Lim, K. Mimura and M. Isshiki, Material Science and Engineering A., **472,** (2007), 235.

58. J.K.O. Asante, J.J. Terblans, W.D. Roos, Applied Surface Science, **252,** (2005), 1674.

59. http://www.marcorubber.com, Macro Rubber (1997 – 2007).

60. K. Jousten, *Thermal Outgassing*, CERN Document Server, Physikalisch-Technische Bundesanstalt, Berlin, Germany, (2000), 111.

61. L. Verheyden, K. Klein, H. Kind, Journal of Scientific Instruments, **1,** (1968), 145.

62. M.P. Seah, Surface and Interface Analysis, **31,** (2001), 721.

63. J. du Plessis and E.C. Viljoen, Applied Surface Science, **59,** (1992), 171.

64. Material-Technologie & Kristalle, Büro für Forshungsmaterialien, Karl-Heinz-Beckurts-Strasse 13, D52428, Jülich, Germany.

65. Goodfellow Cambridge Limited, Cambridge CB4, 4DJ, England.

66. J.J. Terblans, M.Sc. Thesis, University of the Free State, South Africa (2001).

67. E.C. Viljoen, Ph.D. Thesis, University of the Free State, South Africa (1995).

68. H. Giordano, O. Alem, and B. Aufray, Scripta Meterialia, **28,** (1993), 257.

69. H. Giordano and B. Aufray, Surface Science, **307,** (1994), 816.

70. H. Giordano, J.P. Biberian and B. Aufray, Surface Science, **313,** (1994), 266.

71. E.C. Viljoen and J. du Plessis, Surface and Interface Analysis, **23,** (1995), 110.

72. H. de Rugy and H. Viefhaus, Surface Science, **173,** (1986), 418.

73. W.D. Roos and J.K.O. Asante, Surface Review and Letters, **14,** (2007), 1.

74. J.J. Terblans and G.N. van Wyk, Surface and Interface Analysis, **35,** (2003), 779.

75. J.J. Terblans, Surface and Interface Analysis, **35,** (2003), 548.

76. S. Elliot and S.R. Elliot, *The Physics and Chemistry of Solids,* John Wiley and Sons, (1998).

77. S. Stølen, T. Grande and N.L. Allan, *Chemical Thermodynamics of Materials: Macroscopic and Microscopic Aspects,* John Wiley and Sons, (2004).

78. J.K.O. Asante, W.D. Roos and J.J. Terblans, Surface and Interface Analysis, **35,** (2003), 441.

79. J.K.O. Asante and W.D. Roos, Submitted for publication to the Journal Vacuum.

80. G. Gottstein, D.A. Molodov and L.S. Shvindlerman, Interface Science, **6,** (1998), 7

81. K. Lücke and K. Detert, Acta Metallurgica, **5,** (1957), 628.

82. J.W. Cahn, Acta Metallurgica, **10,** (1962), 789.

83. S. Cronjé, M.Sc. Thesis, University of the Free State (2007).

84. C.J. Jafta, W.D. Roos, J.J. Terblans and A.B. Hugo, Instrumentation Science and Technology, **38,** (2010), 261.

85. C. Ryu, Ph.D. Thesis, Stanford University (1998).

86. Y. Takayama, N. Furushiro, T. Tozawa, H. Kato and S. Hori, Material Transactions, JIM, **32,** (1991), 214.

Appendix

Appendix A

Influence of Sb Doping on Grain Growth of

Polycrystalline Cu

A.1   Introduction

The influence of low concentrations Sb doping of Cu polycrystalline samples on the crystal growth and orientation was investigated by optical microscopy and X-ray diffraction (XRD). Doped and undoped samples were annealed at various temperatures and times under controlled conditions. The results show that the average grain size in the Sb doped Cu is smaller by almost a factor of two and that low concentrations of Sb in Cu favours crystallite orientations such as (111) and (420) to the cost of (200), (311) and (222) during annealing. The addition of low concentrations Sb to polycrystalline Cu can be used to influence the electron migration lifetimes and to stabilize the crystal growth of Cu based catalysts, operating at high temperatures.

Grain boundary migration is the basic mechanism of recrystallisation and grain growth in the solid state. During diffusion doping of bi-crystal samples, the mobility of grain boundaries become important. Grain boundary mobility can be influenced by the impurities present, the misorientation of neighbouring grains, and the orientation of the grain boundary plane. In doped materials the mobility strongly depends on the impurity concentration [80].

A.2 Theory

Theoretical approaches by K. Lücke and K. Detert [81] and Cahn [82] are based on the assumption that there is an interaction between impurities and the grain boundary such that the impurities prefer to stay within the grain boundary and, therefore move along with the boundary. As the impurity concentration in the grain boundary increases the boundary moves slower because of a higher activation energy and a concentration dependant pre-exponential factor. The theories predict that the activation energy is independent of impurity concentration and that the pre-exponential factor decreases with increasing impurity content.

A.3 Sample Preparation

Four samples (1 mm thick and 9.5 mm in diameter) were cut from a Cu rod (99.99+ wt.%) and polished to 0.3 μm roughness using a diamond suspension.

Order	Composition	Sample	Anneal	
			Temperature (K)	**Time (h)**
1	Cu	A	-	-
2	Cu	B1, C1	773	1
3	Cu	B2	1173	1
4	Cu + Sb	C2	1173	1
5	Cu + Sb	D	873, 1173	96, 96

Table A.1: The annealing temperatures and times.

The samples (B1 and C1) were annealed for 1 hour at 773 K. This resulted in an average grain size of 20 μm that was visible with the optical metallurgical microscope. A 15 kÅ thick layer of Sb was evaporated onto samples C1 and D. **Table A.1** shows the annealing temperatures and times of the different samples. After annealing, the samples were again polished to 0.3 μm roughnesses and etched. An acidic solution of 1 part HNO_3 and 2 parts H_2O was used [83]. The annealing process in reference [84] was followed. The average grain sizes of the samples were investigated with a Reichart Optical Metallurgical Microscope. The samples were also investigated using a Bruker AXS D8 ADVANCE X-ray Diffractometer with Ni-filtered Cu Kα radiation ($\lambda = 1.5406$ Å). The X-ray tube operating parameters were 40kV and 40mA. The scanning speed was 0.002° per step with a dwell time of 300 ms.

A.4   Experimental Results

A.4.1   XRD Results

Figure A.1 shows the diffraction spectrum of sample A (without annealing). The unusual high intensity of the (111) reflection indicates a preferred orientation of this plane. This result can be attributed to the milling process during the manufacturing of the Cu rod from which the crystals were cut. The intensities of the peaks in **figure A.2**, from sample B1 after a short time at a relatively low temperature (see **table A.1**), is typical of a polycrystalline Cu sample with random orientations. The intensities in the diffraction spectrum of sample B2 (**figure A.3**) that was annealed at a higher temperature, points to a preferred orientation of the (111), (200), (311) and (222) planes. This growth took place at the cost of the (220), (331) and the (420) planes indicating that the surface binding energy of the atoms in the latter orientations is lower than the preferred orientations. It is also reported in literature [85] that

Cu with a (111) preferred orientation has a longer electron migration lifetime as for example Cu with a (220) preferred orientation. It is therefore evident that the electrical conductivity of sample B2 increased. With the addition of Sb to the Cu (sample C), the relative intensity of the (111) reflection increased with approximately 25% (see **figure A.4**). This growth is at the cost of the (222) and the (400) orientations. At extended annealing times the (420) orientation increased further while the (200) and (311) disappears completely (see **figure A.5**). The results show clearly that the addition of small amounts of Sb (< 0.1 at. %) to polycrystalline Cu inhibits the growth of certain orientations such as (200), (311) and (222) and favours the growth of the (111) and (420) orientations.
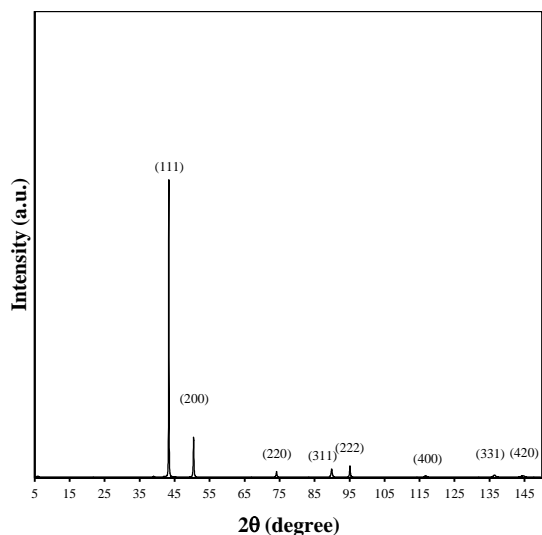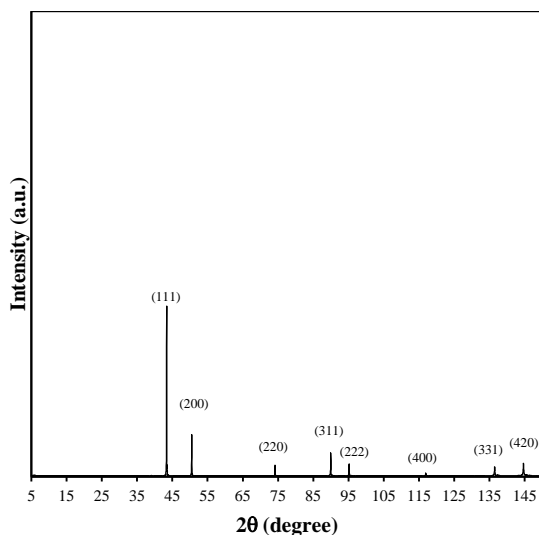
Figure A.1: Sample A as cut from rod.

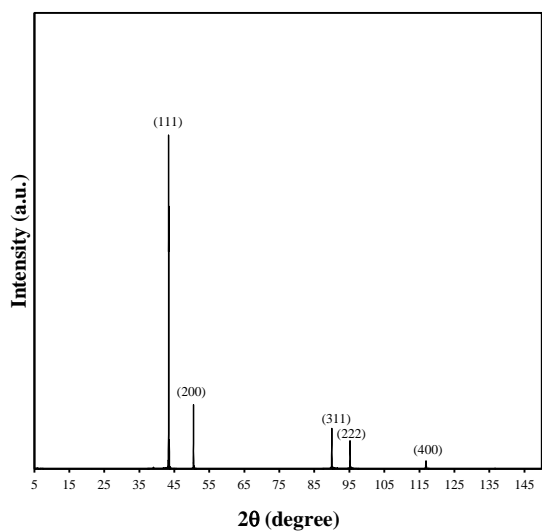**Figure A.2:** Sample B1 that was annealed at 773 K for 1 hour.

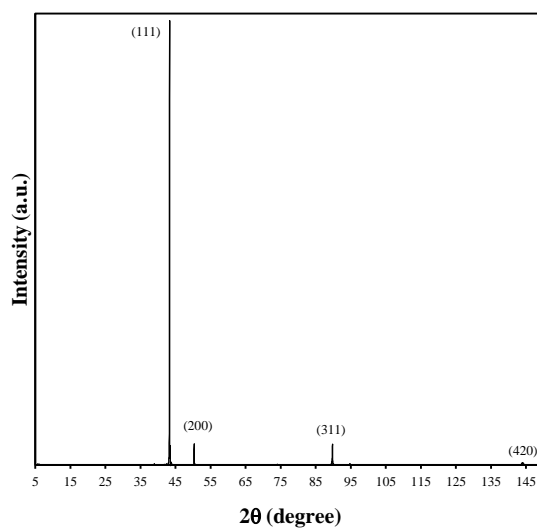**Figure A.3:** Sample B2 that was annealed at 1173 K for 1 hour

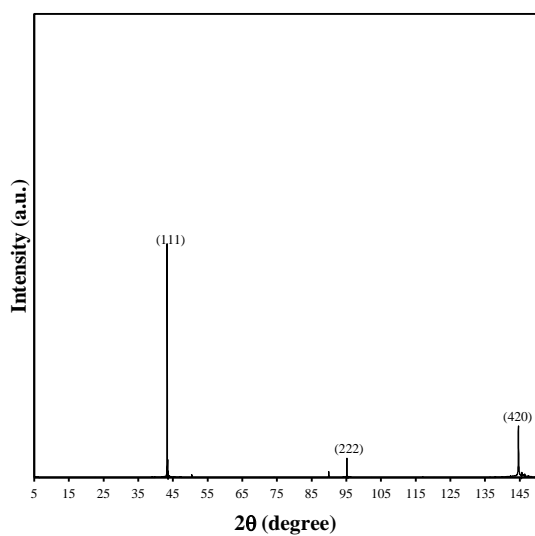**Figure A.4:** Sample C2 that was annealed at 1773 K for 1 hour

Figure A.5: Sample D that was annealed for 4 days at 873 K and 4 days at 1173 K

A.4.2 Optical Metallurgical Microscopy Results

The photos in **figure A.6** show the grain sizes, after annealing (see **table A.1**), of the Cu without any addition of Sb (sample B2) and that of Cu with the addition of Sb (sample C2). The average grain sizes were determined using Heyn's method. This method is described in reference [86]. Two photos from two different areas on the surface of each sample are taken.
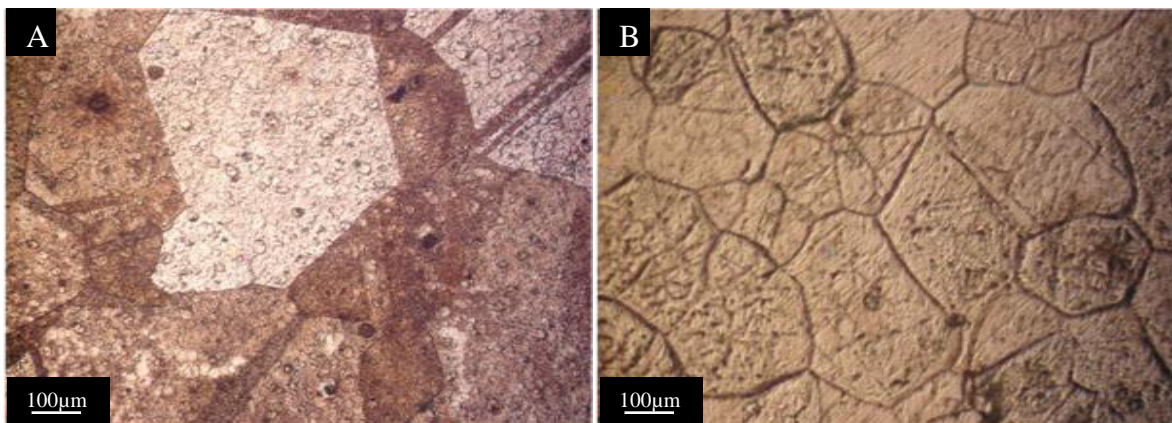

Figure A.6: Optical microscope photos of the etched surface of (A) sample B2 and (B) sample C2.

Sample	Average grain sizes (μm)
A	20
B2	400
C2	250

Table A.2: The average grain sizes of samples A, B2 and C2 for different annealing conditions.

It is clear from the photos in figure 6 and the data in table 2 that the doping of low concentrations Sb has a inhibiting effect on the grain growth of Cu. This was also observed during an investigation of the segregation behaviour of Sb in a Cu bi-crystal, with (111) and (110) orientations.

A.5 Conclusion

The addition of low concentrations (~ 0.1 at.%) Sb to polycrystalline Cu inhibits the crystal growth. This can be used, for example, to engineer the crystal growth of Cu based catalysts, operating at high temperatures, thus maintaining a nano-grain structure. Doping Cu with Sb changes the preferred crystal growth orientation such that the electron migration life time is increased. This can be used to influence the electrical properties of the crystal.